Investigation on Viscoplastic Properties of Au-Sn Die-attach Solder

Tianyi Jin

Technische Universiteit Delft

TU Delft Delft University of Technology

Challenge the future

Investigation on Viscoplastic Properties of Au-Sn Die-attach Solder

by

Tianyi Jin

in partial fulfillment of the requirements for the degree of

Master of Science
in Electrical Engineering

at the Delft University of Technology,
to be defended publicly on Tuesday October 24, 2017 at 15:00 PM.

Supervisor:	Prof. dr. ir. G. Q. Zhang ,	TU Delft
Thesis committee:	Prof. dr. ir. K. M. B. Jansen ,	TU Delft
	B.eng. F de Bruijn ,	Ampleon B.V.
	Dr. ir. R. H. Poelma ,	TU Delft

Acknowledgement

I would like to firstly thank my thesis advisor, prof. Kouchi Zhang at TU Delft, who initially promoted me for this thesis project, gave generous freedom of my own work, and advised me finally to the direction of academic research in following years.

I would also like to thank prof. Kaspar Jansen at TU Delft, who helped me to get results of better quality during DMA measurements.

I am also grateful to the experts from Ampleon B.V. for providing me with all the necessary facilities for the research, and giving significant advice from their rich experience on advanced technology.

I must also thank dr. Rene Poelma as my thesis supervisor, whose office was always open whenever I had trouble in thesis work or had a question in doubt.

Furthermore, I would take this opportunity to express gratefulness to all of the faculty members in TU Delft for their help and support. Without their participation and help, the research could not have been successfully operated.

Finally, I must express gratitude to my parents and friends for the encouragement, support and attention in overcoming numerous obstacles I have been facing through.

Tianyi Jin
Delft, October 2017

Contents

1

Introduction

Reliability is one of the major research topics of modern electronic packaging technology. The characterization of Au-Sn solder fundamental material properties, including viscoplastic properties, are driven by developing tides of studying new lead-free solder materials, and also requested by demand of fast and accurate reliability assessment by industry. This chapter provides background information and the main objectives of this thesis.

1.1. Die-attach Solder in Semiconductor Packages

Rapid development of electronic technology promotes the sustained evolution of human life in recent centuries. In the year 1958 when the very first integrated circuit was developed, the microelectronic technology has been dramatically changing the way of people living in the past decades. A bare silicon chip cannot perform a single function without a package. Being introduced in the final stage of semiconductor fabrication, a package not only physically protects and supports the enveloped silicon die, but also gives possibility of interconnection between silicon die and outer world. In some cases the package also fulfill a function of the heat sink or an optimized footprint for the convenience of system-level manufacture. Package types are classified into a great deal of international standards to meat various requirements of electronic devices.

Die-attachment is one of the major steps of some silicon chip packaging, when the diced silicon die (or sometimes multiple dies) is mounted to a supporting substrate via a bonding layer, or the die-attach material (Figure 1.1). The die-attach bonding layer provides two major functions:

- Physically fixation between silicon die and packaging substrate
- Heat dissipation of heat generated by silicon die

In low cost and low power devices glue or epoxy adhesive are often used as the bonding media. Nevertheless in high power devices the silicon die will be attached by alloy materials such as alloy solders or sintered metal since it requests higher fatigue resistant materials with good thermal, electrical and mechanical performance. In the following part of this thesis, all solder discussed refers to die-attach bonding solder, instead of other applications, and the study will also be driven by die-attach applications.

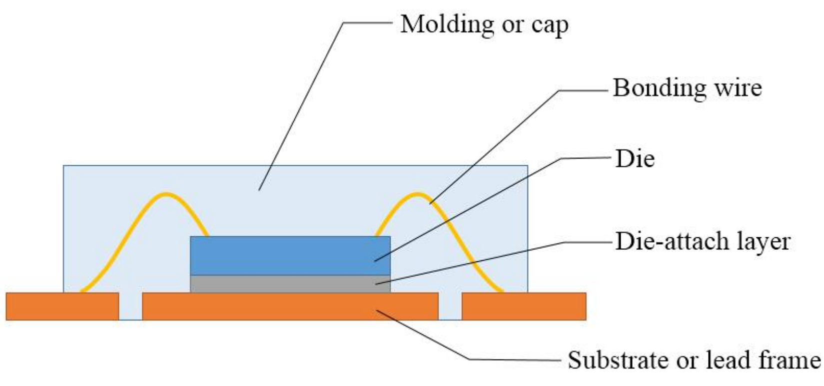

Figure 1.1: A typical chip packaging with die-attach layer

1.2. Au-Sn Solder and Fabrication Process

Research on new Pb-free die-attach solders is driven by the pressure of environmental restrictions and also pushing requirements of performance by industry, especially on applications for harsh working environments. For many decades the Au-Sn solder system has been attracting research interests for its natural advantages of high stability and performance on high operating temperature, and being considered as relatively hard solder with better creep resistance, compared with other Pb-free solder system such as Sn-Ag-Cu(SAC). Au-Sn is one of the preferred Pb-free solders for high power density devices, for advantages of:

- High melting point(280°C)
- High creep resistance
- High thermal conductivity(58W/mK)
- Excellent corrosion resistance
- Good soldering wettability on many surface treatments

The Au-Sn solder allows flux-less soldering because of the minimal surface oxidation of the high content of gold(Au), thus low cost and fast soldering process without the use of flux could be performed in vacuum or under forming gas [1]. Therefore the Au-Sn solder system is widely used in flip-chip die attaching products in power electronic and opto-electronic [2][3].

Au-wt%20Sn(29.0 atomic percent Sn) eutectic alloy is the most common used solution, which has melting point at 280°C. This composition is widely utilized for the reason that the solidified alloy is formed at phase transition point(Figure 1.2) between two steep liquidize lines to provide favourable soldering and bonding performance [4]. A typical process temperature from 300°C to 320°C provides rapid liquidus period as well as fast solidification to effectively shorten the solder processing time. A high melting point also gives possibility for subsequent process using other Pb-free solder with lower melting point over Au-Sn soldered component, such as board level assembly of die-attached devices, or following packaging process that needs to be operated at high temperature. Almost all studies on Au-Sn solder are based on this composition for its wide industrial utilization. In this work, Au-Sn refers to Au-wt%20Sn unless indicated otherwise.

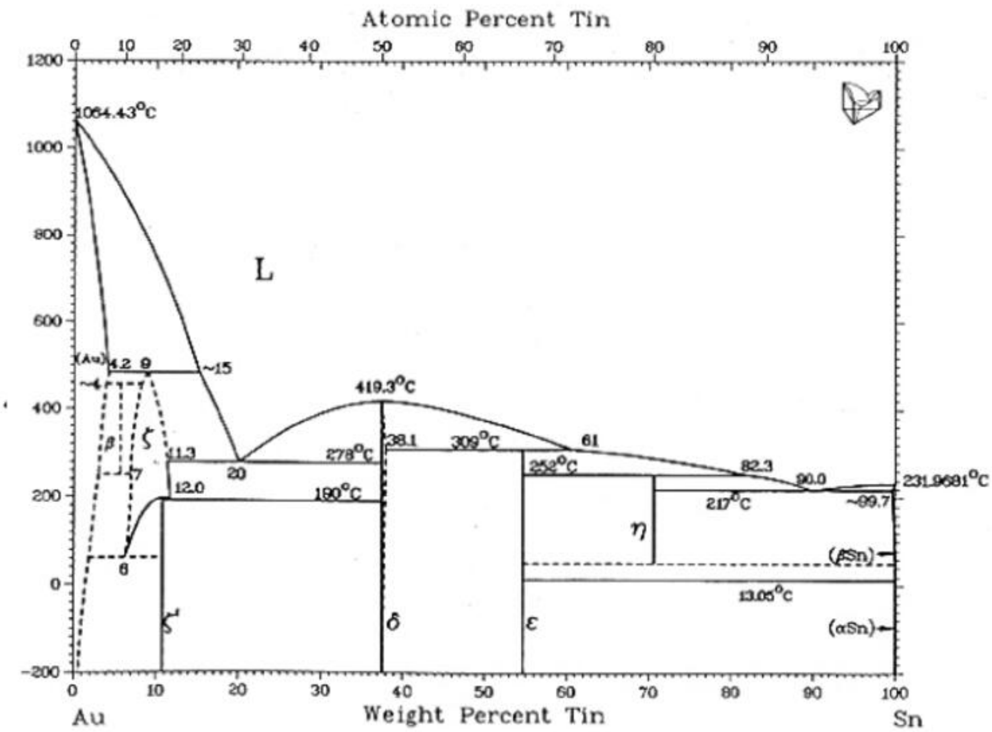

Figure 1.2: Phase diagram of binary Au-Sn systems [5]

Deposition and reflow are two major steps of Au-Sn die-attachment processes. Since solder wire or foil are no longer favoured because Au-Sn is relatively brittle compared to other Pb-free solders like SAC, solder preform is a conventional technology to deposit Au-Sn. Gold(Au) and tin(Sn) components are mechanically mixed, where the particle scale can be range from several micrometers to hundreds of micrometers for different purposes of use, even nano-particle paste is sometimes used for special applications. The mixture then is moulded into preforms with tailored dimensions. In most cases no flux or additives is added into Au-Sn preforms. This technology allows Au-Sn to have desired shape before soldering process, to increase the consistency of products.

Advanced technology such as electroplating provides a more cost effective alternate, by applying less material(especially for expensive gold) in faster process speed and higher material availability, and it has already been introduced into volume production [6][7]. A layer of gold and another of tin are electro-plated sequentially then reflow process is directly taken to form eutectic alloy, where interdiffusion condition induces microstructure variability [8]. This deposition technology provides lower inner-stress, better uniformity and less risk of oxidation impurity [9].

No matter what type of deposition method is used, the Au-Sn solder needs reflow process, in which the deposited Au-Sn is heated above its melting temperature than cooled down to solid, bonding between a silicon die and a packaging substrate. Programmed reflow profile including temperature controlling and ambient gas configuration is used to achieve better soldering performance.

1.3. Solder Reliability Assessment

Fast growing of electronics competing market requires short research and develop duration for new products, thus a rapid reliability assessment for microelectronic packaging is highly demanded. Accelerated life test(ALT) is introduced as a common methodology for lifetime prediction in electronics industry. By applying laboratory tests with specified harsh conditions, ALT reduces the test time from real-life test conditions but still give accurate lifetime prediction on basis of several failure modes, such as strain energy accumulation and crack propagation which often heavily determine the total lifetime of the entire product. A typical thermal-mechanic accelerated life test for power electronic chips is achieved by a series of thermal cycling tests(Figure1.3). Additionally, with the help of finite element analysis(FEA) the industry now has a strong tool to rapidly predict lifetime of devices by simulating thermal cycling tests, and to improve the lifetime performance during package design phase.

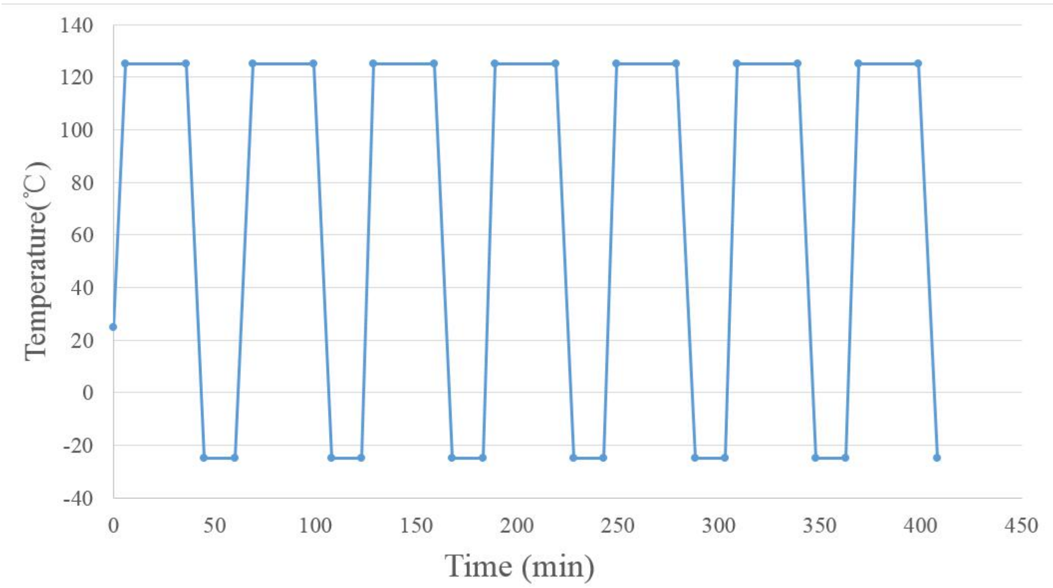

Figure 1.3: A typical test temperature profile for packaging lifetime prediction

Material properties, especially viscoplastic properties characterization is one of the most significant topic to solder material fundamental study, which also has great value for reliability assessment. It is known as rule of thumb that the creep behaviour becomes notable when temperature exceeds half of the melting point(in Kelvin). As mentioned, for its superior properties at high temperature, the 280$°C$ melting point Au-Sn solder has been applied for many years in power electronic and optoelectronics, where operating temperature often reaches up to 175$°C$. In these conditions, viscoplastic performance has dominant influence on total thermal-mechanic response of the die-attach solder, and failure modes like strain accumulation and crack propagation might be heavily influenced by solder viscoplastic response.

1.4. Challenges for Die-attach Solder in Electronics Packaging Technology

Although Pb-free solders including Au-Sn have been brought to market for several decades, challenges remain in modern electronics packaging technology that require further study. Following closely to these existing challenges the value and objectives of investigations in this work are established.

1.4.1. Fundamental Investigation of New Pb-free Solders

Being accused as potential dangerous and harmful materials, Pb(Lead)-based solder system is no longer favoured by industry after decades of popular since strict environmental requirements were pushed by Restriction of Hazardous Substances(RoHS) and Waste Electrical and Electronic Equipment(WEEE) in EU countries since 2006, that Pb-free materials are musts during electronics manufacturing and assembly to be certified as green products. Figure 1.4 indicates during last decade the fast decrease in using of Pb-based solders, and on the contrary the rapid increase in using of Pb-free solders. In some countries, traditional Pb-based materials are even banned from use in certain applications. Conventional packaging process uses Pb-Sn, Pb-In-Sn or Pb-Ag-Sn systems as die-attach solder materials. Not satisfied the environmental requirements, these Pb-based solder systems lost market share against new generation of Pb-free solders, such as SAC, Bi-based or Au-Sn systems. There always lies challenges under a huge growth of Pb-free solders, when new materials were developed continuously to fulfill growing industrial needs. Though Au-Sn has been applied to electronic industry for many years, it is still a rather new type of solder that has not been studied as intensively as other transitional Pb-based solders or early-applied Pb-free solders, and does not have such systematic study of their fundamental properties as conventional Pb-based solders, not to mention even further research that taking microstructure effects into consider. Great deal of scientific value lies on the fundamental study of material properties, including viscoplastic properties, of evolutionary new solder materials.

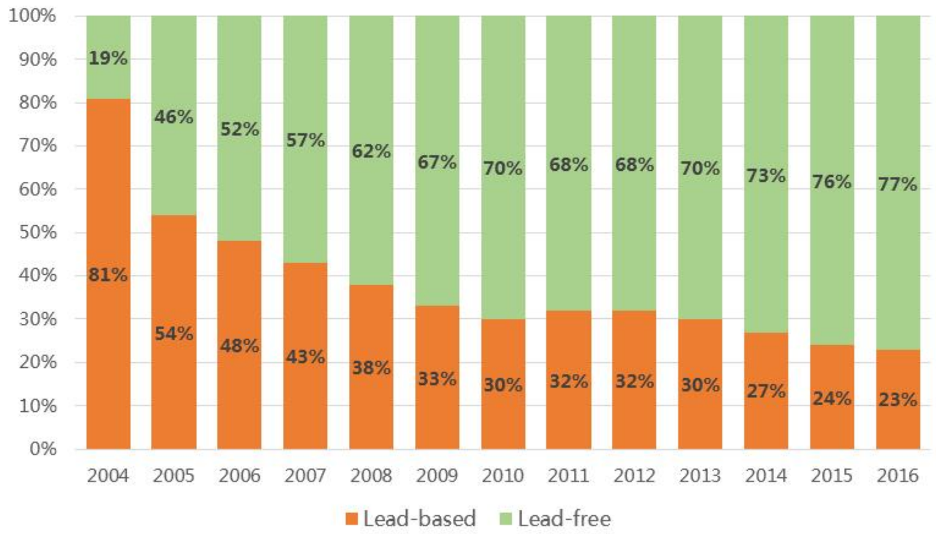

Figure 1.4: Historical Trend in Proportion of Lead-free Versus Lead-based Solder Consumption Worldwide. (Source: 2016 IPC Global Solder Statistical Program and Global Solder Market Report)

1.4.2. Material Characterization Method for Fast Reliability Assessment

Au-Sn solder is broadly used as die-attach material for high power electronics, such as solid state lightning, power electronics, radio frequency electronics or laser optoelectronics, which always have common features like high operating temperature, heavy duty-time and frequently switching. These harsh operating features can potentially shorten device lifetime by triggering multiple failure modes of die-attach solders. Many efforts have been made to study failure mechanism and fatigue models of die-attach structures, since the reliability of packaging is increasingly important in industry of mass production power electronic devices, and huge price will be paid for any failure or break-down in these application inevitably. With the help of finite element analysis(FEA) the industry now has a strong tool to rapidly assess lifetime of devices, which rests on various of numerical models describing material properties. Figure 1.5 shows a typical IC product development procedures where simulation-based reliability improvement becomes a significant step among process of designing new products.

Mechanical properties, including viscoplastic properties characterization is the centerpiece of building mechanical models especially for die-attach solder materials. For manufacturers of electronics using Au-Sn die-attachment, the Au-Sn raw material is very likely bought from supplier rather than self-fabricated. Most reflow profiles are recommended by solder supplier by considering soldering feasibility, product reliability and process economics, after experiments of raw materials. However due to many reasons, the actual solder in products might have very different properties, which means it is very necessary for manufacturer willing to gain best soldering performance to have customized solder characterization with tailored preference on their products. Nevertheless, challenges exist when other side effects like microstructure effect might appear under certain circumstances and need to be considered. There is not a standard characterization method regarding the microstructure variation effect on mechanical properties for Au-Sn solder, especially the viscoplasctic properties, which makes it extra difficult to accurately evaluate product reliability by using FEA simulations. Being highly demanded by industry, an accurate characterization method for solder material properties always contributes to industry values, or in long-term view as economical values.

1.5. Research Objectives

The main object of this thesis project is to investigate on viscoplastic properties of Au-Sn die-attach solder while considering microstructure

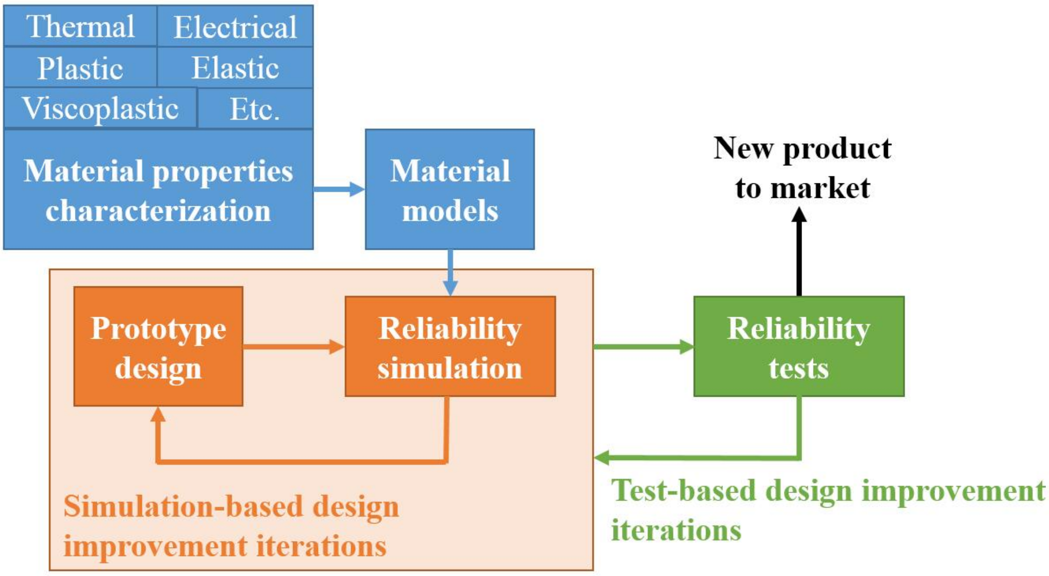

Figure 1.5: A typical development logistics for IC product reliability improvement

as an effect factor, by analyzing data from a series of mechanical experiments, and conclude the investigation by a group of viscoplastic models. To fulfill the goal, following objects need to be achieved:

Establish a reliable method for Au-Sn solder viscoplastic properties characterization and modelling

Develop a consistent experimental method to authentically observe and precisely measure the viscoplastic behaviour of Au-Sn solder. The experiment data must contribute to a viscoplastic model system that ought to agree with real experimental result and has practical value to be adopted in reliability assessment.

Investigate microstructure effect on Au-Sn solder viscoplastic properties

Develop a consistent method to control Au-Sn solder microstructure and apply mechanical experiment upon different microstructures. Explain the influence on viscoplastic properties using materialogy theory for Au-Sn solder. Build viscoplastic models for Au-Sn solder with different microstructures, and compare the lifetime predictions corresponding to different microstructures.

1.6. Outline

This following thesis consists four parts: a chapter that provides fundamental of Au-Sn solder properties and a theoretical methodology of characterize its viscoplastic properties; a chapter explains a detailed experimental based methodology that is able to characterize Au-Sn solder's viscoplastic properties, including raw material introduction, test specimen preparation, shear creep experiments and test data analyze; a chapter presents a study of microstructure effect on Au-Sn solder viscoplastic performance by experiments and following analysis; and summary chapters consist conclusion and suggestions for future work.

2

Viscoplastic Models of Au-Sn Solder

As a new Lead-free solder, Au-Sn solder has been widely used in many heavy-duty applications as die-attach material, for its unique excellencies in many properties, including viscoplastic properties. Theories are given to support characterization from measurement to convincing models. This chapter provides a theoretical methodology for characterizing its viscoplastic properties.

2.1. Introduction

Mechanic properties have been heavily studied for solder materials to predict their reliability behaviours even before the devices existing. It is important to study viscoplastic properties of solders that are used in high power density applications, because the harsh thermal-mechanical environment these applications can potentially meet. Currently in industries constitutive models simulated by finite element analysis(FEA) is popularly used as tools to predict thermal-mechanical behaviours such as strain-stress response and lifetime assessment, where the numerical models are acquired from standard tests on materials. A good thermal-mechanic viscoplastic model helps the industry to design robust products or improve manufacture processes to achieve higher economical value by estimation of product lifetime with better accuracy. Therefore it is necessary to build a methodology of characterize solder viscoplastic properties. Creep models are often used to describe viscoplastic properties of material, by connecting multiple mechanical variables, such as strain, stress, temperature and time, with one or a set of equations. Most classic creep models are built subjectively to match experimental data. With more studies being carried out on this subject, new models with more capability were introduced.

2.2. Solder Viscoplastic Properties

Solder material properties have been divided into time-independent elastic component, time-independent plastic component and time-dependent viscoplastic component. Viscoplasticity is described as the phenomenon that solid objects have non-elastic, time-dependent deformation under constant mechanical stress, or time-dependent stress relaxation under constant strain deformation. The phenomenon is also named as creep behaviour, while the non-elastic, time-dependent strain is also named as creep strain. The phenomenon occurs when the object is under tensile, compressing or shear stress. Figure 2.1 shows a typical strain-time curve for solder alloy under constant tensile or shear stress. Behaviour of strain against time in Au-Sn solder is expected to be clearly observed in three main stages [10]. The time-domain strain curve starts at a certain level of non-time dependent elastic and plastic strain. Then a very short primary creep stage reflects a rapid decrease in strain rate after the very beginning of creep. The strain rate then becomes steady when it has decreased to a certain level, entering the steady-state creep stage, or also known as secondary creep stage. The stable strain-rate will finally lead to a large strain that strain rate suddenly rapidly rises until an rupture occurs, which means the solder joint is mechanically broken.

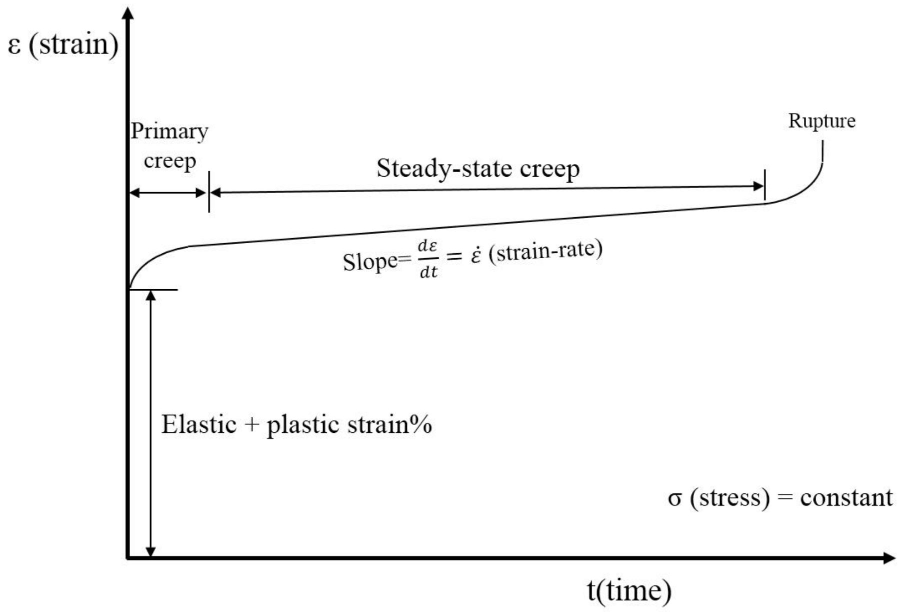

Figure 2.1: Strain versus time curve for Au-Sn under constant shear stress

The *Burger's* model is able to well describe solder's three-stage strain versus time curve, where material elastic, rate-dependent plastic and viscoplastic strain are well fitted into one Equation 2.1:

$$\epsilon_b(t) = k_0 + k_1 t + k_2(1 - exp(-k_3 t)) \tag{2.1}$$

The *Burger's* model simplifies the creep mechanism into three elements in parallel, including a spring element representing elastic response, a dashpot element representing steady-stage creep response, and a frictional element representing primary creep response (Figure 2.2). The equation form is a sum of three terms, where k_0 is the non time-dependent term refers to total elastic strain and pure plastic strain, k_1 refers to the steady-state creep strain rate during secondary creep stage, and the last non-linear term indicates the non-linear primary creep strain.

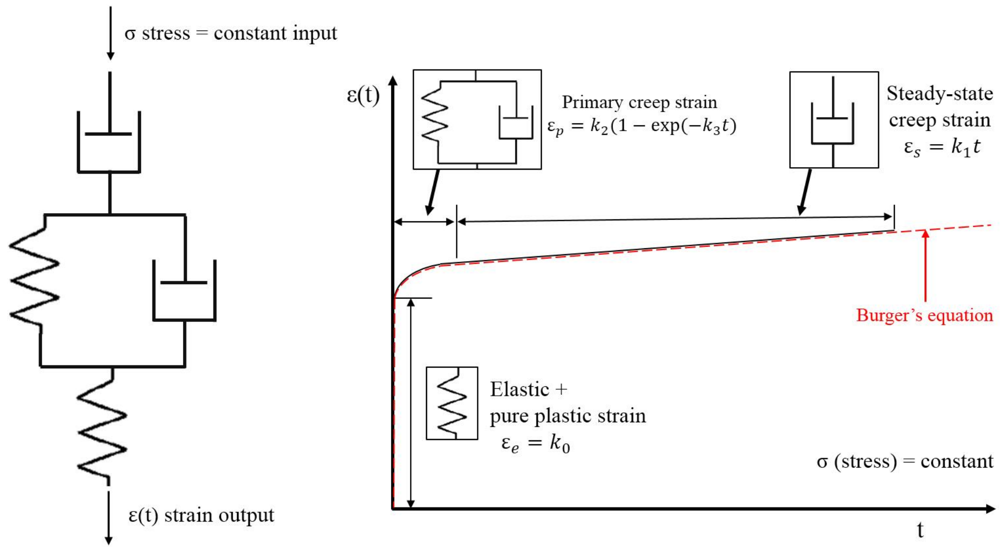

Figure 2.2: The *Burger's* model and three-stage viscoplastic strain-time response

From the view of materialogy, although the precise mechanisms are not completely clear, dislocation climb and grain boundary sliding are deducted as two major mechanisms of viscoplasticy in solder alloys.

Dislocations are defects in crystal lattice structure, including edge dislocations and screw dislocations. When shear stress inside the material exceeds critical resolved stress, dislocation slip occurs and develops an increase of dislocation density, until dislocations may not slip after reaching the grain boundary due to orientation. The piled up dislocations have to climb to another slip plane by atomic spacing. This process leads to time-dependent plastic creep deformation, and the rate of steady state dislocation movement increases exponentially with increasing temperature in a certain range of stress. Significant literature exists supporting dislocation slip and climb assisted with core diffusion is one of the dominant creep mechanisms in SAC solder [11][12][13]. The mechanism of void formation involves grain boundary sliding, which occurs under the action of shear stresses on the boundaries, when grain boundary sliding and grain decohesion caused creep deformation is the dominant mechanism leading to thermo-mechanical fatigue in some lead-free solders [14]. Researches revealed that the grain boundary sliding is one of the major creep mechanisms in Pb-Sn solder [15][16], and similar result was also given in Au-Sn solder by Zhang et al. [17]. Nevertheless, not all viscoplasticy mechanism is constant when dominant mechanism could switch, or becomes as the combination of several mechanisms under specific conditions such as microstructure, temperature or stress level.

2.3. Viscoplastic Models

2.3.1. Classic Creep Models

As stated previously that a typical creep strain-time response has three main stages. Elastic response has individual principle that is non time-dependent, so as plastic response. Both two non time-dependent responses are not described in time-dependent creep models, but by individual elastic models and plastic models. Primary creep stage exits in very short time, and the creep rupture only happens at extremely large strains which is far from realities of die-attach application that total creep response is dominated by steady-state creep stage. Thus following classic creep models only take steady-state creep into consider. And they are the most adopted models in creep behaviour studies of solder materials.

To describe steady-state creep behaviour, the classic *Bailey-Norton's law* [18], or sometimes called power creep law, is commonly used to fit the general experimental results for solder materials [19][20][21][22]. The equation has a simple format as Equation 2.2

$$\dot{\epsilon} = A\sigma^n \tag{2.2}$$

where $\dot{\epsilon}$ is the steady-state creep strain-rate, σ is the stress, A is a scaling constant and n is the stress exponent. Both A and n are expected as temperature dependent parameters. The power law reveals the most fundamental exponential relationship between stress and creep strain-rate. However it has limitation that the power law does not reveal any connection between creep behaviour and temperature.

In the work of Zhang et al. [17] and Elmer et al [23], the *Weertman-Dorn* model [24] is used to fit the solder creep behaviour, which is defined as Equation 2.3

$$\dot{\epsilon} = A\sigma^n exp(-\frac{Q}{RT}) \tag{2.3}$$

The equation is developed from *Bailey-Norton's* law, where Q is the activation energy of the deformation, R is the gas constant, and temperature T is brought into consideration. Then *Garofalo* model [25] was also introduced to comparison, which is defined as Equation 2.4

$$\dot{\epsilon} = A[sinh(\alpha\sigma)]^n exp(-\frac{Q}{RT}) \tag{2.4}$$

where hyperbolic sine function and a coefficient α are introduced to correct the fitting under very high stress condition. The result of the work shows both models are able to provide better fit of Au-Sn creep behaviour under certain temperature conditions, and *Garofalo* model has a better agreement with experimental data due to a lower variance of error. Furthermore, Liu et al [26] explains in their work when n is between 3 and 7, the creep deformation is attributed to dislocation climb and glide. Other creep models such as *Larson-Miller* [27], *Manson-Haferd* [28], *Monkman-Grant* [29], are based on the similar principle of *Norton's* law but add adjusting parameters to have better agreement with experiment data.

Parameters of these classic creep models can be obtained by non-linear fitting with data groups of creep strain-rate $\dot{\epsilon}$, applied stress σ and temperature T from a series of tensile or shear experiments on tested solder samples. But these models have limitation of focusing on steady-state creep stage, and ignoring primary creep stage that also contains viscoplastic information.

2.3.2. Anand Viscoplastic Model

The *Anand* model [30] is a constitutive model to describe the inelastic behaviour including rate-dependent plastic and creep response under high homogeneous temperature, giving a better fitting for experiment results, when both primary creep and steady-state creep are described. The equation of *Anand* model is defined as Equation 2.5

$$\dot{\epsilon} = A[sinh(\xi\frac{\sigma}{s})]^{\frac{1}{m}}exp(-\frac{Q}{RT}) \tag{2.5}$$

where an internal variable s and stress scaling coefficient ξ are introduced on basis of classic equations. s is defined by a set of evolution equations as Equation 2.6

$$\begin{aligned} \dot{s} &= h_0|1-s/s^*|^a \cdot \frac{1-s/s^*}{|1-s/s^*|} \cdot \dot{\epsilon}, a > 1 \\ s^* &= \hat{s}[\frac{\dot{\epsilon}}{A}exp(\frac{Q}{RT})]^n \end{aligned} \tag{2.6}$$

where h_0 is the hardening constant, a is the strain rate sensitivity, s^* is the saturation value of s and $\hat{s}$ is the coefficient value. The evolution equation has an extra initial condition of $s(0) = s_0$, where s_0 is the initial value of s at initial time $t = 0$. Classic creep models have limitation in describing complex viscoplastic functions, nevertheless complex evolution models like *Anand* model was not applied in practical use until computation ability has been strongly enhanced thanks to computer science growth since 70s, which promises new opportunity and challenge to investigate complex viscoplastic models. When FEA has been gradually used to predict the reliability behaviour of mechanical structures, yet the viscoplastic model is often involved into simulation only after the model is input as user-defined codes, which is very complicated and time consumptive. To solve this problem, some FEA tools has pre-load viscoplastic model code to avoid complex user-defined settings. The very complex *Anand* model is already available in commercial FEA software, and has been often used in solder mechanical simulations corresponding to reliability assessment [31][32][33]. However it seems limited literature exists that *Anand* model is used to investigate Au-Sn solder viscoplastic properties.

In total nine parameters are needed to determine the *Anand* model: $A, Q, \xi, m, h_0, \hat{s}, n, a$ and s_0, where the stress scaling coefficient ξ is always set to a constant. Parameters of *Anand* model can be differed due to variation of experimental design or data fitting methods. The parameters can be determined from experiment data of creep tests, where a series of creep strain ϵ versus time curves are measured under various of applied stress σ and temperature T. The determination of model parameters steps are:

1. Measure creep strain versus time curves under multiple stress and temperature conditions by standard tensile or shear tests.
2. Fit each strain versus time curve with *Burger's* model(Equation 2.1).
3. Obtain strain-rate versus time curves by differentiating *Burger's* equations.
4. Obtain all parameters by fitting strain versus strain-rates curves to math deducted Equation 2.8 with corresponding stress and temperature data [33].

$$\epsilon = \frac{1}{c_3(A^{-a}\dot{\epsilon})^n}[\{c_2(A^{-1}\dot{\epsilon})^n - \frac{\xi}{sinh^{-1}(c_1 A^{-1}\dot{\epsilon})^m}\}^{1-a} - \{c_2(A^{-1}\dot{\epsilon})^n - s_0)\}^{1-a}] \tag{2.7}$$

where

$$\begin{aligned} c_1 &= e^{(\frac{Q}{RT})} \\ c_2 &= \hat{s}\{c_1\}^n \\ c_3 &= (a-1)h_0(c_2)^{-a} \end{aligned} \tag{2.8}$$

3

Viscoplastic Properties Characterization for Au-Sn Solder Based on Shear Creep Tests

This chapter provides an experimental methodology that is able to characterize Au-Sn solder's viscoplastic properties. Furthermore including raw material introduction, test specimen preparation, shear creep tests procedures and test data analyze are explained. At the end a validated viscoplastic model of tested Au-Sn solder is given.

3.1. Introduction

As stated in Chapter 2, experimental data of creep tests, where a series of creep strain ϵ versus time curves are measured under various of applied stress σ and temperature T, is required to derive a viscoplastic model of Au-Sn solder. In die-attachment application, shear stress is more likely to occur on Au-Sn solder when silicon die and packaging substrate often have coefficient of temperature expansion(CTE) mismatch. Therefore a viscoplastic model under shear stress condition is preferred for solder applications. Standard test procedures are often used for study mechanical properties of common metal alloys. However there is no existing standard test used in this project for testing Au-Sn solder mechanical properties for following reasons;

In commercial application the scale of the Au-Sn joint is often limited as BGA solder balls with diameter of tens of μm, or a thin die-attach film with a few μm thick and a few mm in length and width, which will possess very different physical performance compared to bulk standard test specimens. The reason is assumed by existing studies that reveal the Au-Sn microstructure has heavily dependency on size-effect. In the work of Hutter et al. [34], different sizes of Au-Sn solder bumps were observed to have various microstructure geometry in cross section and achieved different electrical yield performance in fatigue tests. The microstructure of μm-scale Au-Sn solder joints has been studied by Yoon et al. [9], which shows the phase distribution in Au-Sn joint is non-homogeneous with irregular-shaped coarse grains. The grains of a single phase might scale up to $10\mu m$, thus under realistic applications Au-Sn solder might not be considered as eutectic of a general composition as bulk materials. That is to say, the microstructure effect can not be negligible with μm-sized materials, like a thin layer of Au-Sn. Therefore, to perform accurate mechanical analysis for Au-Sn die-attach solder, parameters from characterization tests upon similar scale of specimens are considered more reliable than conventional bulk-based standard tests.

Classic dog-bone tensile specimens or V-notched beam shear test specimens are majorly used in standard metal viscoplastic property characterization, which is normally in mm-scale of length, width and thickness. However considering the major content is pure-gold, the Au-Sn solder is no doubting an extremely costly material. It is not realistic for experiment operators to fabricate bulk Au-Sn specimens in large amount, and neither to ask material supplier to mold specimens in tailored dimensions.

Therefore instead of standard test with bulk size specimens, characterization must be taken by Au-Sn specimens with similar dimensions to its realistic applications. That is to say, the Au-Sn solder in experiments ought to have a geometry of very thin layer that its thickness should be in range of 5 to 50 μm. In this work, Au-Sn preform films in certain dimensions were sponsored. Then constant stress creep test profile is used on test specimens, and information of Au-Sn solder including creep strain ϵ versus time curves are measured under various of applied stress σ and temperature T.

3.2. Experiment Preparation

3.2.1. Specimen Design

As it is stated above, it is not only a obligatory but also a preference that the scale of test specimens should be similar to actual application to approach the real response. In this work a shear test set-up for Au-Sn solder viscoplastic properties characterization is designed, where a single shear test specimen consists two flanges and one Au-Sn preform, as shown in Figure 3.1. SOT1250 ACP flanges were used as shear force conductors and test joint supporters. In following part of this work flanges or copper flanges refer to the SOT1250 ACP flanges. The flange has physical geometry parameters as shown in Figure 3.2. It is generally used in mass production of SOT1250 ACP packages as package substrate. The flange has a core of pure copper(Cu) which is considered to be rigid: high elastic Young's modulus, high plastic yield stress and very high creep resistance. In ideal single side shear tests, parallel shear force are operated on both sides of test Au-Sn joints. And the shear force conductors should be ideally rigid materials to avoid false read-out of set-up deformation. Among others it is also very essential to have the creep deformation of flange under experimental temperature negligible.

The flanges have surfaces firstly coated with a 10μm layer of silver(Ag)

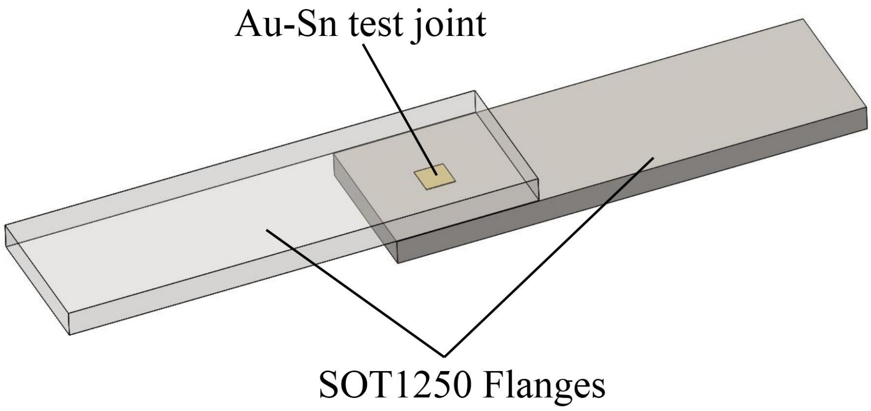

Figure 3.1: Shear test specimen with Au-Sn preform and two flanges

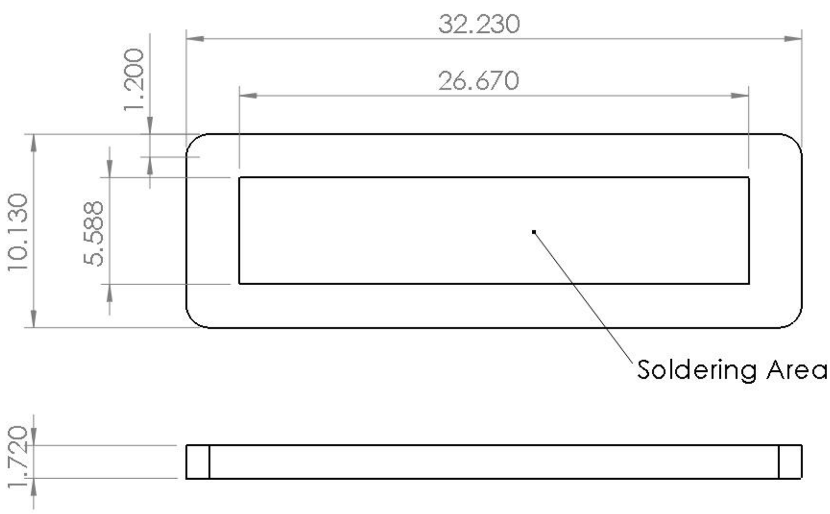

Figure 3.2: SOT1250 ACP flange dimensions

as a stress relief layer, then a thin 0.5μm layer of nickel(Ni) to prevent atom diffusion against sliver layer. On top of nickel layer is fine coated with 30-100nm palladium(Pd) then 3-12nm gold(Au) to give better soldering wettability and also prevent surface oxidation. Two surface treatment profiles are operated respectively on two sides: on top side, where die and die-attachment are located, the middle area of flange, or so called soldering area, is treated to have very fine surface roughness(maximum bump size less than 1.5μm) and high flatness(maximum flatness tolerance within 0.01905mm), to achieve better soldering performance and consistency. Other area on top surface has less treated surface roughness that maximum bump size is less than 12.5μm. The bottom surface is unused for die mounting or any other electrical connecting, therefore the whole surface has less treatment for cost saving, thus the fine-treated area on top surface was used as soldering area. All flanges were cleaned before shipment therefore no extra cleaning is needed before sample preparation.

The tested Au-Sn solder raw material was chosen in a form of pre-manufactured thin films, or so called preform. In the rest of this work, Au-Sn preform refers to Au-Sn raw material before sample fabrication. The Au-Sn preform dimension was designed as 0.079 x 0.079 x 0.002 $cubicinch$(or 2.000 x 2.000 x 0.050 mm^3) manufactured by *Corning*. The reasons this dimension was chosen are:

- to have good operability during manual specimen assembly, where preforms need to be manually picked and placed by tweezers
- to have large margin of cross section area when the specimens need to be sliced and examined under microscope for microstructure observation
- to have rather small shear area that the shear stress will be high enough to initiate obvious creep deformation in short test time

It is rather necessary to mention that the Au-Sn preforms should be placed in a sealed package in cool, dry environment where direct sun is kept out, to avoid contamination and extra oxidation on surfaces. Figure 3.3 shows a Au-Sn preform on bottom flange with align holes.

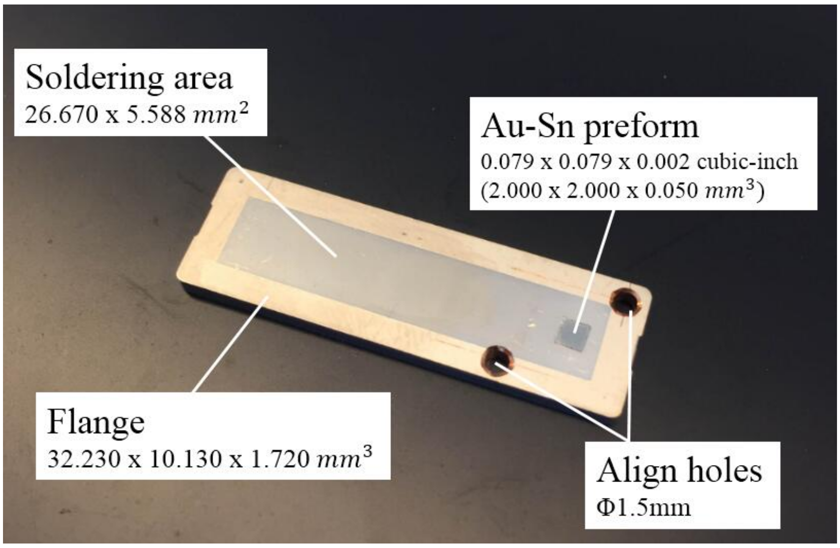

Figure 3.3: Dimensions of Au-Sn preform on bottom flange with align holes

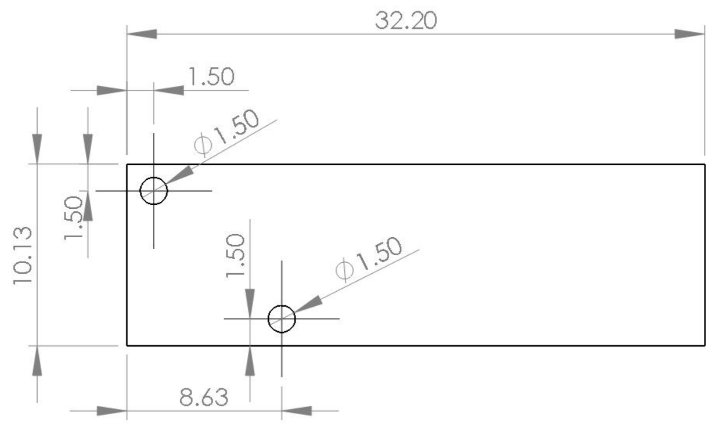

Figure 3.4: Dimensions of align holes in flanges(unit: mm)

Single shear test requests that the shear forces on two sides must be applied in parallel during whole test process. And it is also very hard to measure joint height for all specimens before or after test, when joint height is a must parameter for creep strain rate calculation. This is requesting that two flanges must be perfectly aligned to parallel with each other for any specimens, and the distance between two flanges must be controlled in advance during specimen preparation. Any misalignment of flanges causes uneven distribution of shear stress at Au-Sn joint area, or brings peeling force component to pure shear test. A feasible and consistent specimen prepare process was operated in this work, where a specially designed jig and spacer films are introduced. Flanges need to be modified before they are assembled to test samples. Align markers were precisely curved on the flange surface, where two align holes were drilled through. Drawing design of the align holes and final appearance of align holes are shown in Figure 3.4. These holes would be used as align markers of sample assembly.

3.2.2. Specimen Preparation

In Figure 3.5, the fabrication of shear test specimens are listed in 8 steps:

Step 1 Clear any glitch or particles in align hols

Step 2 Place bottom flange through two align pins and on the align jig

Step 3 Place Au-Sn preform in soldering area by tweezers

Step 4 Put spacer films on bottom flange and dummy flange

Step 5 Place top flange through two align pins and on the spacers

Step 6 Place weight on the top flange

Step 7 Carefully load the set up into reflow oven, and run programmed reflow profile

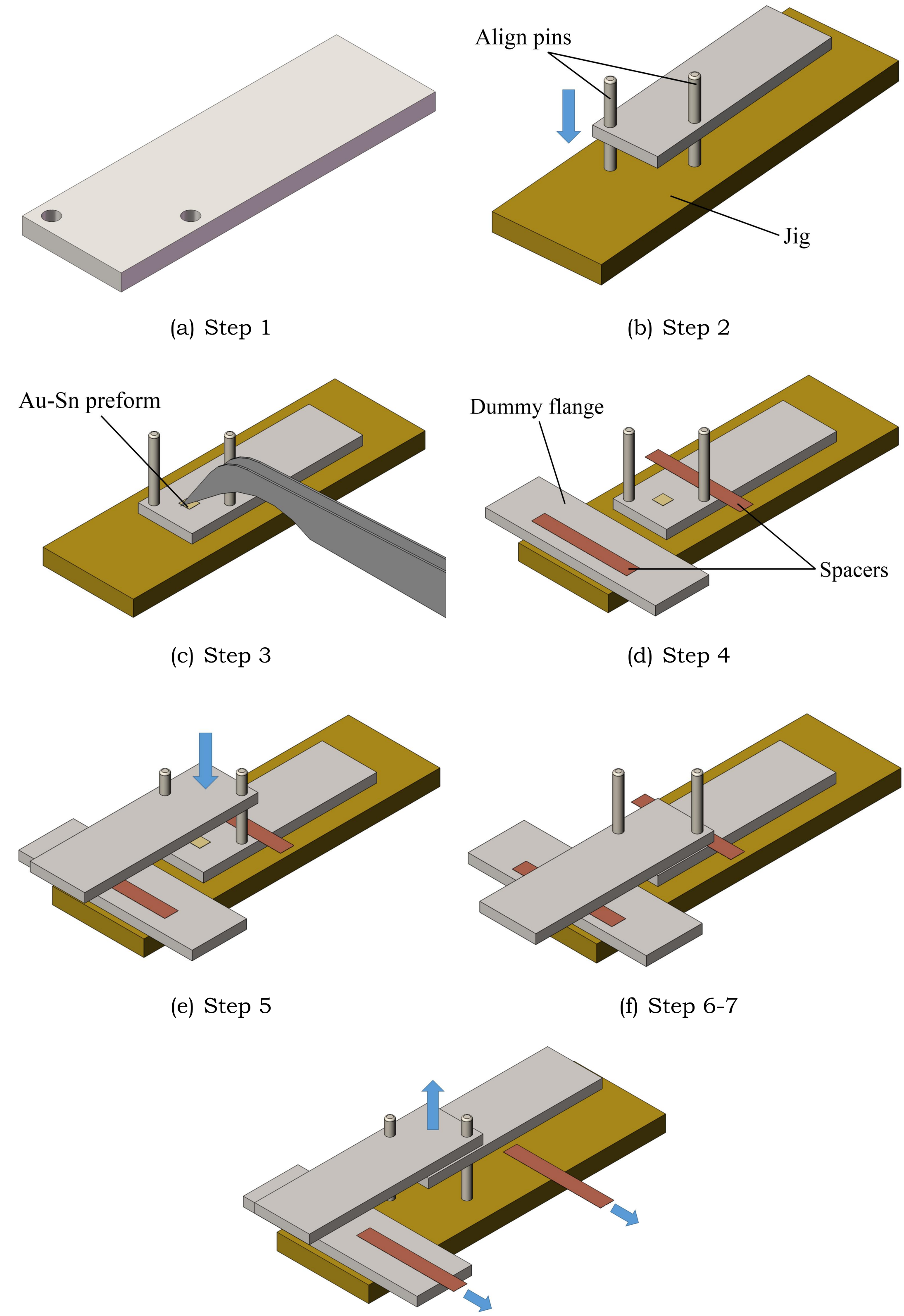

(a) Step 1 (b) Step 2 (c) Step 3 (d) Step 4 (e) Step 5 (f) Step 6-7 (g) Step 8

Figure 3.5: Preparation procedures of Au-Sn shear creep test specimens

Step 8 Unload the set up, remove the jig, spacers and dummy flange

A jig is designed to make alignment of two flanges(Figure 3.6). It is made of a piece of pure copper(Cu) which has larger dimensions than flanges. Two steel pins were riveted onto the copper piece and could perfectly match the align holes on flanges. These two parallel mounted align pins are able to fix two flanges during assembly. The diameter tolerance of align pins and holes is controlled below 10%. Spacer films and dummy flanges are introduced to control the joint height among all specimens. The spacer films are pure copper(Cu) thin films in constant thickness, which is 40μm in this work. The dummy flange is same as flanges being used in specimens, and supports the top flange to have parallel alignment during reflow process. Weight is used to give vertical pressure on top flange so that spacer films are properly pressed and kept flat. In this work the weight was three flanges providing 15 grams gravity weight, which was determined by experience from experts. The assembled set-ups ready for reflow process are shown in Figure 3.7.

Thermal expansion during reflow process was also a necessity to be considered. Several trial tests showed that the holes will choke align pins due to thermal expansion of pin and shrinking of the hole, which enhance the security of flange fixing. The copper expansion among jig, flanges and spacer contributes to a joints thickness increasing of 0.2μm, or 0.5% relative error in thickness, when maximum temperature during reflow process could go up to 320°C. The reflow process would be operated in reflow oven SRO702/704 (Figure 3.8). The reflow oven provides an hermetically sealed and iso-thermal chamber where temperature can be precisely programmed by profile input. Chamber atmosphere could either controlled to vacuum or certain type of supplied gas.

In mass production of using Au-Sn preform as die-attach material, a certain reflow temperature profile is used. The profile consists eight phases that each phase has its own purposes. The temperature and gas configuration profile is shown in Figure 3.9 where reflow phases

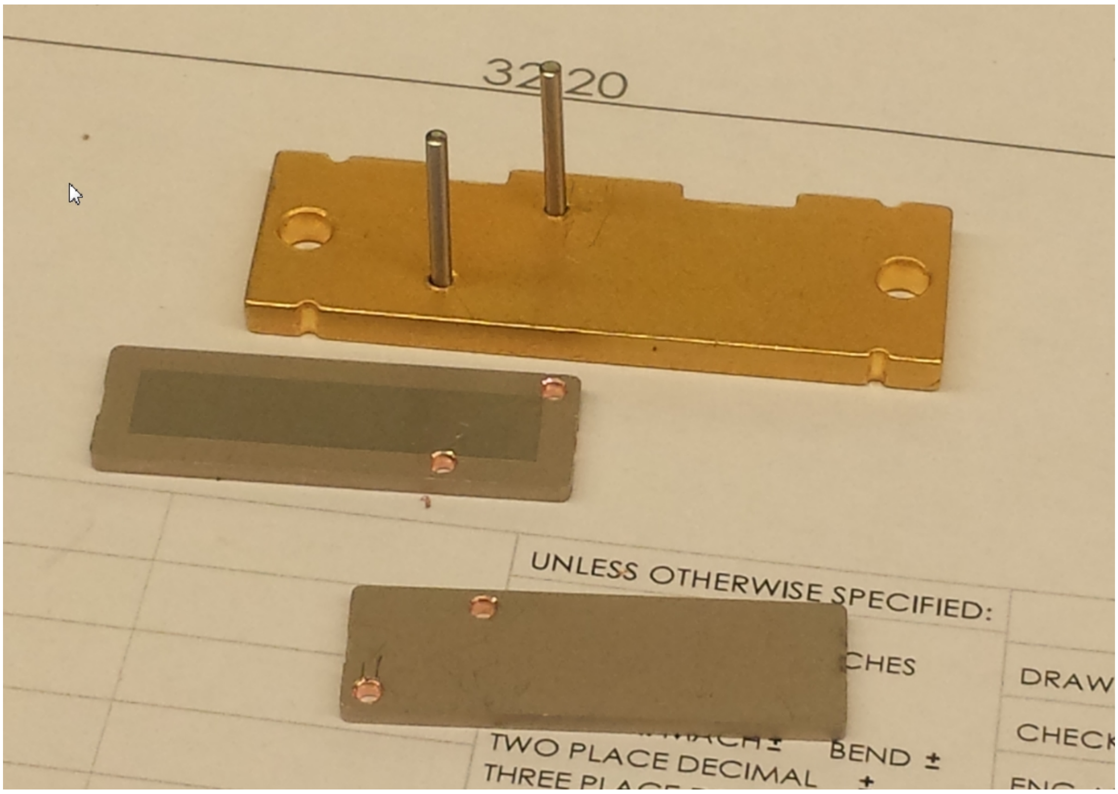

Figure 3.6: A jig with two align pins and two copper flanges with matching align holes

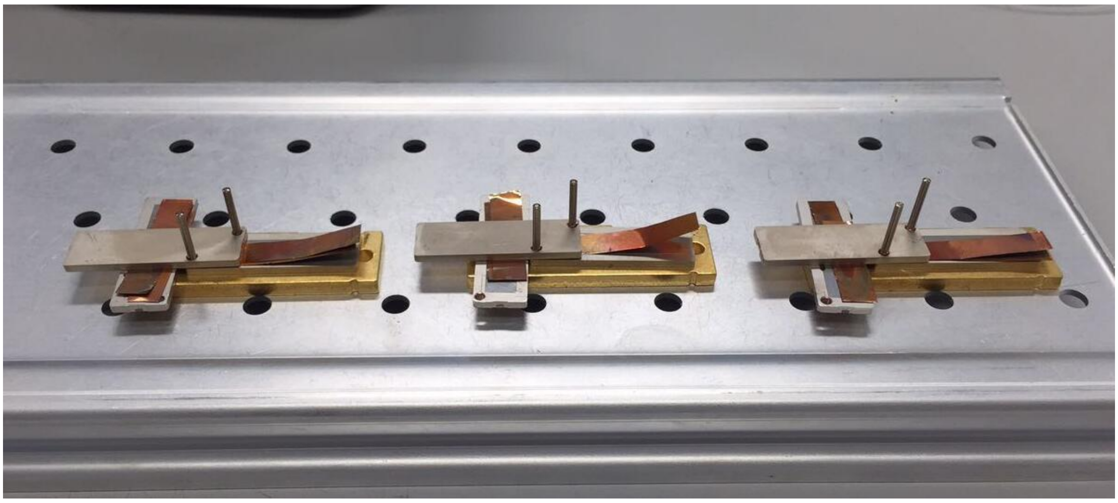

Figure 3.7: Specimen set-ups ready for reflow process

Figure 3.8: Reflow oven SRO702/704 used in sample preparation

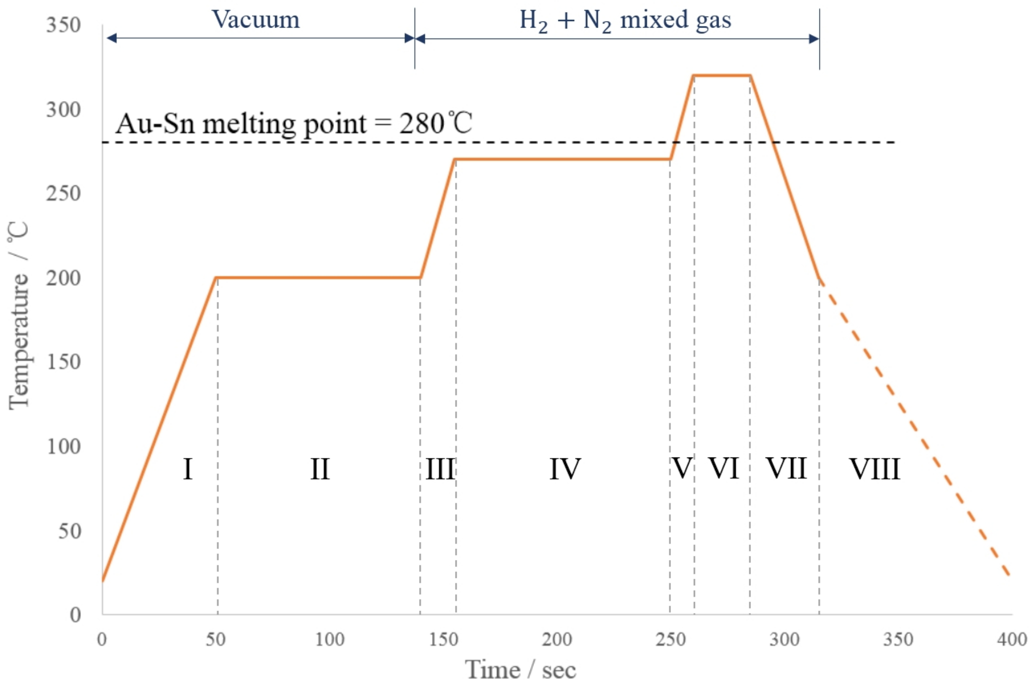

Figure 3.9: Reflow temperature and gas ambience profiles

are marked as (I) to (VIII). Key parameters are specified: heating rate is 3K/sec, temperature above liquidus(TAL) is 40°C, ramp rate is 3K/sec and rapid cooling rate is 4K/sec. This standard profile is also used in mass manufacture of products with Au-Sn solder in die-attach process. Besides reflow temperature profile, it also requires pressure during reflow process to prevent voids in the solder, however high pressure occasionally causes edge flaws or push the solder out of the die edge, even damage the die [35]. Thus nowadays Au-Sn reflow process is mostly carried out under vacuum then reductive atmosphere mixed gas of hydrogen and nitrogen, with efficient lower pressure to suppress oxidation layer to form [36][37][38].

(I) Fast heat from room temperature to 200°C, heating rate is 3K/sec.

(II) Temperature stays at 200°C for 90 seconds, vacuum the chamber.

(III) Fast heat to 270°C, heating rate is 3K/sec, charge reduction gas (mixed of hydrogen and nitrogen) to reduce surface oxidation.

(IV) Temperature stays at 260°C, wait 105 seconds for fully oxidation layer reduction.

(V) Fast heat to 320°C, heating rate is 3K/sec, Au-Sn preform starts to melt and wets the soldering surface.

(VI) Temperature stays at 320°C for 25 seconds, Au-Sn preform melts into liquid state.

(VII) Cool the chamber to 270°C in programmed rapid cooling rate of 4K/sec, charge nitrogen gas to maintain cooling rate. Total TAL time is 48.3 seconds.

(VIII) Open chamber and cool the specimens down to room temperature by air convection.

After reflow process the align jig and spacers are detached from the specimen. The preform melts and forms a thin layer of Au-Sn joint between two flanges. The joint is so brittle that the specimens need to be kept in cases with cushioning foam pads to avoid joint cracking before shear tests. Figure 3.10 shows prepared specimens ready for shear tests.

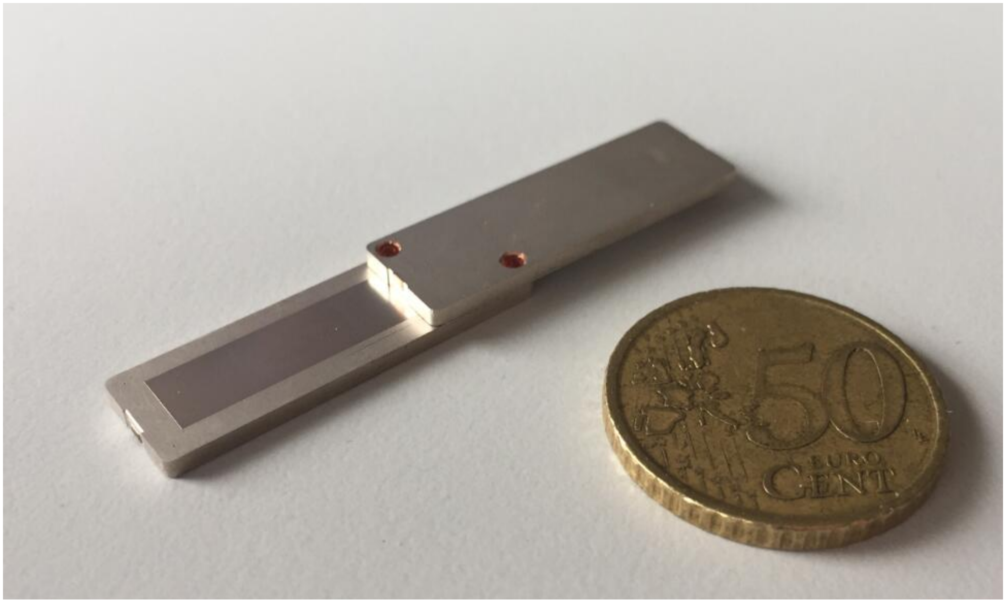

Figure 3.10: A prepared Au-Sn specimen for shear creep tests

3.3. Experimental Procedures

3.3.1. Dynamic Mechanical Analyzers(DMA)

The shear creep test will be operated by *TA Instruments* Q800 Dynamic Mechanical Analyzers(Figure 3.11) with capability listed in Table 3.1. DMA gives possibility of measuring mechanical properties as functions of time, frequency and temperature, on various types of material like metal or polymer. DMA is commonly used by scientific researchers as well as industrial users for material characterization or performance tests. DMA provides high accuracy displacement measurement with very fine precision up to $1nm$. It has also been used in viscoplastic property studies on various solders.

Figure 3.11: TA Instruments Q800 Dynamic Mechanical Analyzers(DMA)

Maximum Force	18N
Minimum Force	0.0001N
Force Resolution	0.00001N
Strain Resolution	1 nanometer
Frequency Range	0.01 to 200Hz
Temperature Range	-150 to 600C°
Heating Rate	0.1 to 20C°/min
Cooling Rate	0.1 to 10C°/min
Isothermal Stability	±0.1C°
RH Control	Yes

Table 3.1: Q800 DMA capabilities and specifications from user manual

The active shaft is the active part in DMA, which is driven by electromagnetic motors and floating on non-contact air bearings. This allows the shaft to be active with little friction and less momentum lag. Test samples fixed at active shaft, are also fixed by an alternative clamp on the other side. A certain clamp is chosen to full fill one of mechanical tests: tensile, double-side shear, compress or 3-point bend. In this work only standard tensile clamp was used(Figure 3.12). DMA also has a furnace chamber that allows measurement under controlled temperature or humidity profiles. The furnace is made of iso-thermal material to secure temperature stability in the furnace.

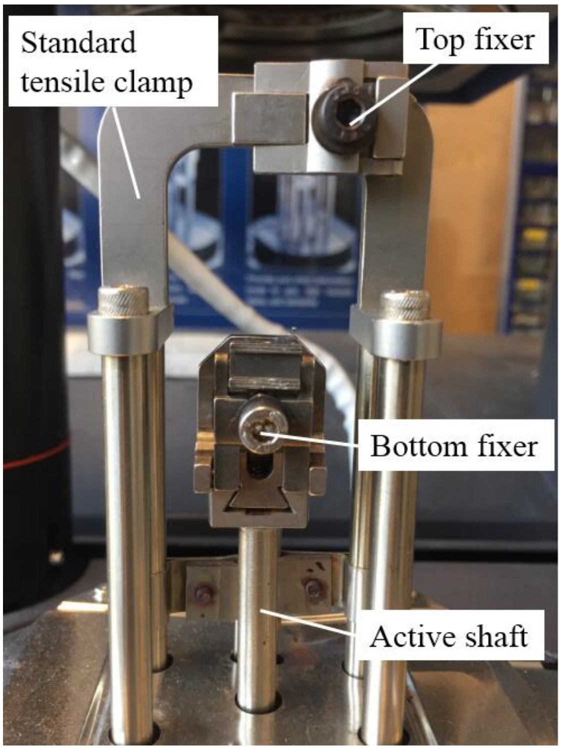

Figure 3.12: DMA standard clamp and active shaft

3.3.2. Shear Creep Test Methods

Two flanges of one specimen were respectively fixed at the active shaft and clamp(Figure 3.13). The fixer of active shaft can be slightly shifted horizontally to align with flanges, making sure that the shear movement is parallel to flanges. It is sufficient to do the alignment by naked eye because the air bearing gives the shaft a tilting margin of several degrees that the shaft is able to automatically compensate slight misalignment. Fixer on active shaft was tightened before tightening clamp fixer, to avoid risk of break specimen from applying too much tightening force while the shaft fixer could still be moving. The furnace was closed and locked when specimen was secured by both fixers.

”Creep-and-hold” DMA test profile is shown in Figure 3.14. For fresh load tests, i.e. the specimen is just loaded to DMA set-up and the furnace needs to be heated from room temperature to set temperature, there was a period of 20 minutes for thermal equilibrium, to ensure the whole set-up has uniformly distributed temperature. For non-fresh load tests, i.e. the specimen has just finished a test session and immediately starts next test session, the thermal equilibrium time is reduced to 5 minutes, reasons being the Au-Sn microstructure might change due to exposing in high temperature especially in 175°C and 200°C tests, or in other words to reduce thermal annealing effects. It is worth noticing that a very low pre-load force(F=0.010N) was applied during thermal equilibrium period. This pre-load force is taken for pre-tightening all potential clearances between set up and fixers or in electro-magnetic motors. Before applying shear creep tests on Au-Sn specimens, a dummy test was taken that guaranteed no creep was detected on flanges or equipment under test conditions.

After thermal equilibrium period a programmed load force was applied on active shaft. To avoid step shock of shear force, which might generate vibration and inertia displacement, the force loading and unloading were programmed to linearly increase from pre-load force to set force and decrease to pre-load force both in 1 minute. Load force stopped increasing when it reached set hold force. The active shaft position was precisely recorded afterwards, which indicates the shear creep displacement. The creep hold time was 30 minutes for 125°C, 175°C and 150°C tests since under lower temperature Au-Sn has lower creep rate, therefore it needs longer time to observe and record significant information. The creep hold time was reduced to 20 minutes in 200°C tests to avoid thermal annealing effects. Shaft displacement, load force and tempera-

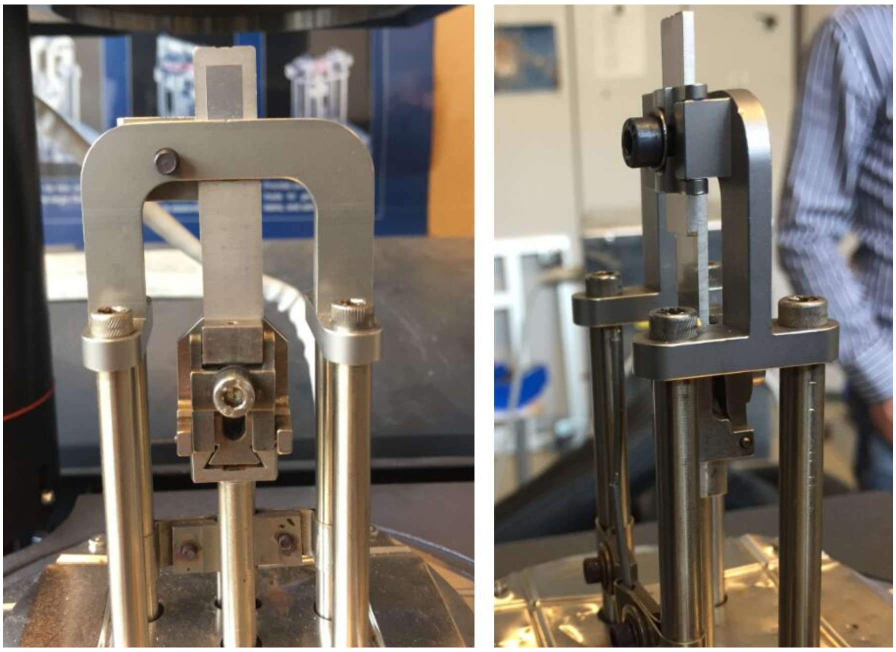

Figure 3.13: Test set up on DMA clamps before shear tests

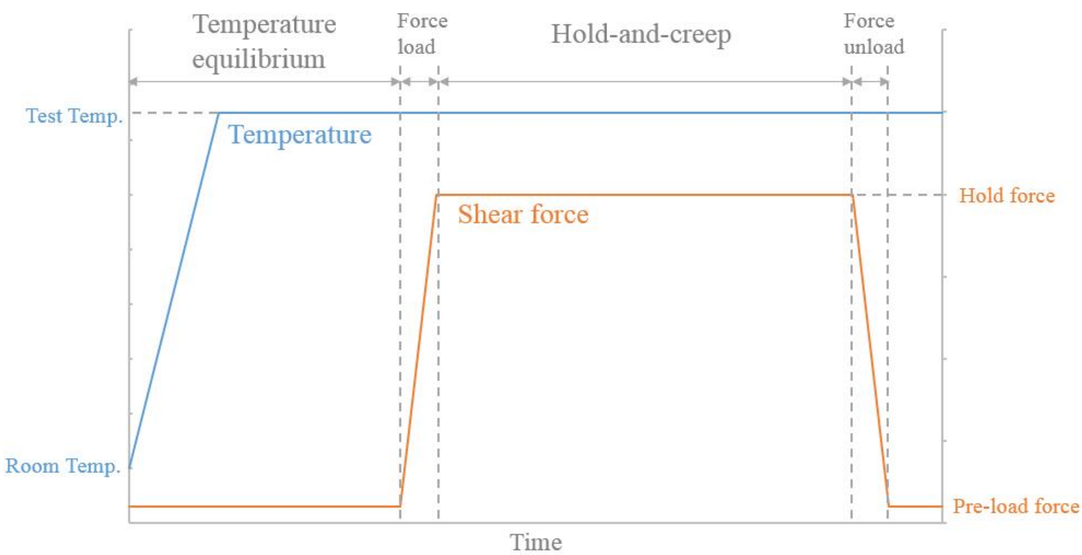

Figure 3.14: DMA force and temperature profiles of shear creep tests

ture data were recorded every second. Figure 3.15 shows one of the test output curves, where the test was done under 175°C and load force was 18N.

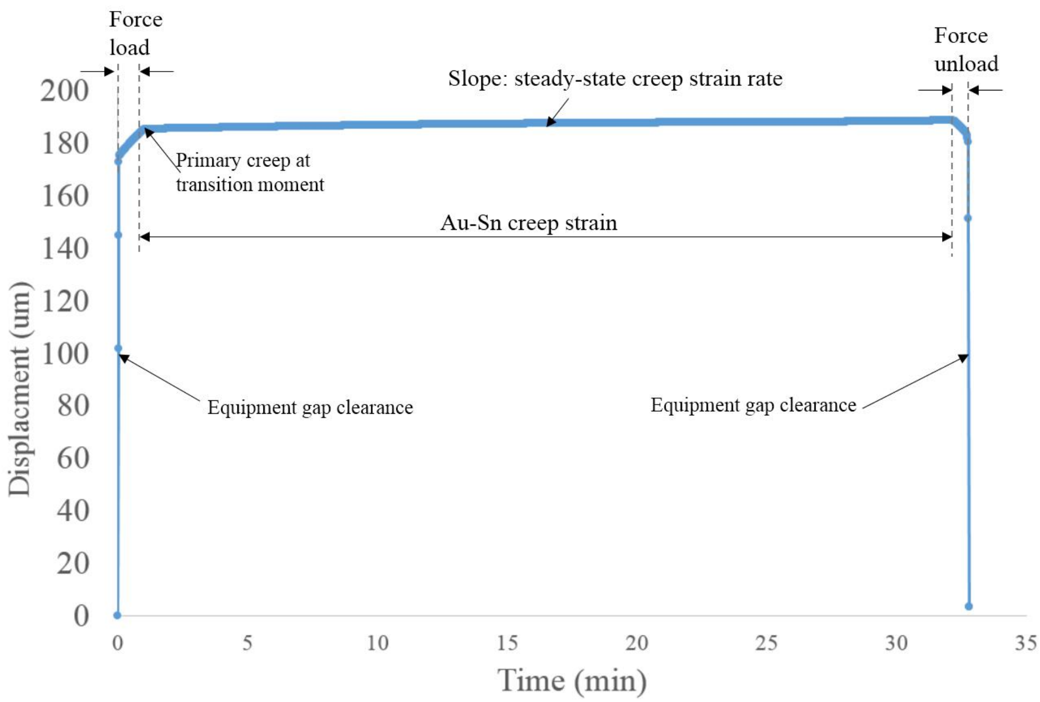

Figure 3.15: DMA output: shear displacement versus time of test(F=18N, T=175°C)

Two large step responses occur at the moment that shear force starts to load or unload. It is caused by clearance between the test sample and clamp fixers, or slight clearance in DMA air bearings. During very short force loading and unloading steps, the total deformation increased or decreased almost in linear which can be considered as time-independent deformation. However not only the deformation of Au-Sn test joint was recorded but also other time-independent deformation of the flanges, clamps and active shafts, which has similar spring factor($k \approx 10^7$). That is to say, the time-independent element of Au-Sn test samples were not able to be measured. Inevitably, part of primary creep strain occurs in force load step, but the loading speed is set fast to reduce the overlap period. Steady-state creep deformation was recorded during force hold-and-creep step, and the slope, or creep rate was close to constant as expected. It is necessary to point out that some tests, especially at low shear force, a reduction of deformation is observed in steady state stage(also seen in Figure 3.19), which indicates a strain drop or even sub-zero strain. It is not very possible that the sample shrink when applied shear force, but probably because the force was too low to resist external influence, such as temperature drifting or vibrations.

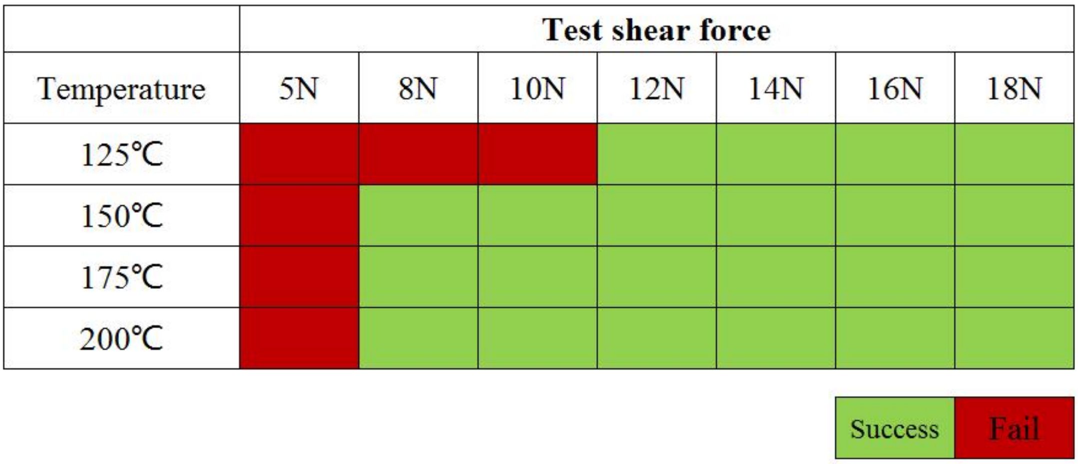

Figure 3.16: Full factorial DoE of 28 tests: 5 tests failed, 23 tests succeeded

A reasonable Design of Experiment(DoE) is able to effectively reduce test workloads while maintaining sufficient information extracted from experiments. Full factorial DoE provides maximized information from tests by covering all combinations of factors. Considering test workloads and equipment capability, a full factorial DoE of 4 temperature conditions and 7 shear force conditions was used. Figure 3.16 shows total 28 full factorial tests done. Where 5 of 28 tests failed(in red) for not having sufficient information of creep strain-rate, because at these tests the shear force applied was too low to generate obvious creep strain in limited test time, and the deformation slope was hidden or mixed with equipment error. Eventually 23 of total 28 tests gave usable data.

3.4. Experiment Result and Analysis

DMA output contains time t, shaft displacement Δd, load force$F$ and temperature T data. Data processing is needed to extract required creep strain, creep strain-rate and shear stress information by Equation 3.1.

$$\begin{aligned} \epsilon &= \frac{\Delta d}{h} \\ \dot{\epsilon} &= \frac{d\epsilon}{dt} = \frac{1}{h}\frac{\Delta d}{dt} \end{aligned} \tag{3.1}$$

where creep strain ϵ is determined as division of displacement Δd and joint height h, which is $40\mu m$ that was controlled by spacer films in specimen preparation process. And creep stain-rate is deducted as the slope of displacement versus time curve divided by joint height. The strain-rate value is adopted as the average slope of total creep time, while experimental errors are also taken from minimum and maximum average slope of 3 minutes during total creep time.

$$\sigma = \frac{F}{A} \tag{3.2}$$

Shear stress is determined as shear force F dividing solder joint area A(Equation 3.2). Nevertheless it is impossible to measure the solder joint area until the specimen is broken. Although the Au-Sn solder preform has a regular shape, the solder is still possible to move in liquid state because of surface tension, external vibration or displacement of the set-up, which results the solder joint irregular in shape, and difficulty in calculating solder area. As shown in Figure 3.17, the irregular area size was measured by counting pixels from SEM images after deliberately breaking the specimen. The value was averaged by multiple measurements, and error bars indicate maximum and minimum measured result. To simplify the calculation, engineering area was used, where the stress is assumed to be constant during deformation, instead of being slightly differed due to shear area or thickness changes as true stress.

Figure 3.17: Au-Sn solder joint area measurement by counting pixels from SEM images

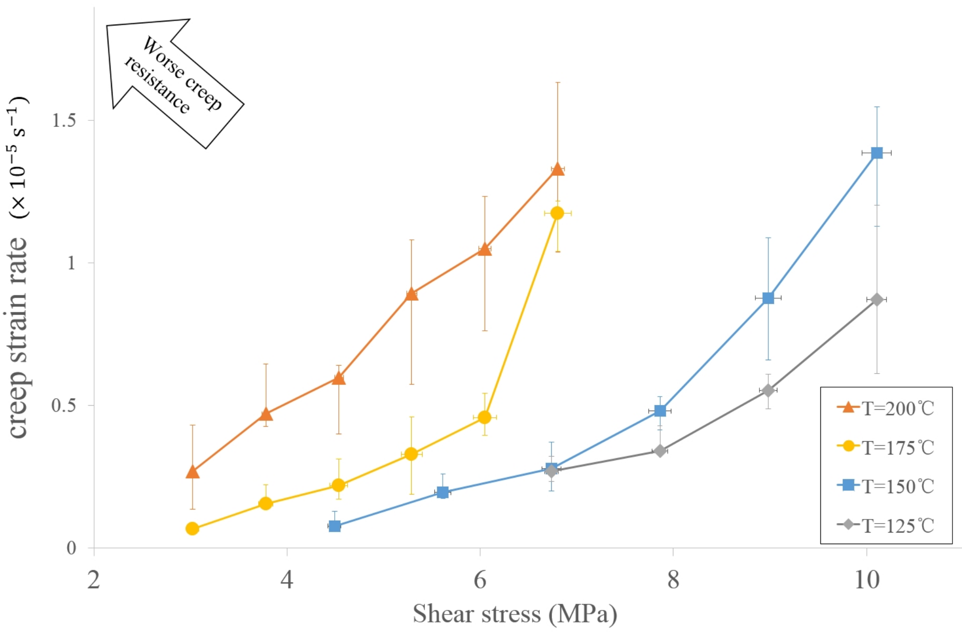

Figure 3.18: Au-Sn creep strain-rate versus shear stress under different temperature conditions

Processed data from the shear creep test of Au-Sn solder is shown in Figure 3.18. The creep strain-rate shows exponential feature against shear stress, and separation against temperature. The data is sufficient for building classic creep models or advanced *Anand* viscoplastic model.

3.5. Numerical Procedures

3.5.1. Model Parameter Fitting

The viscoplastic properties of Au-Sn can be well described by *Anand* model, and its parameters can be determined by a series of creep tests, which were performed in previous sections. Following the steps stated in Chapter 2, all strain-time curves were firstly fitted in form of Burger's equation(Equation 2.1). Since the full factorial experiment consists more than 20 sets of data, only the fitting process of one group of tests are shown as an example. Figure 3.19 shows strain versus time plots from experiment at temperature of 175°C, and the dot lines indicate fittings for Burger's equation. And processed strain versus strain-rate curves are shown in Figure 3.20, where dot lines indicate the result of Equation 2.8 fitting. Non-linear aggression method was used to determine the parameters of *Anand* model. Iterations are taken in other data groups with different test temperature for the sake of goodness of fit that correlation coefficient(r-square) during fitting process were all above 0.8. The determined parameters for *Anand* model are listed in Table 3.2. It is necessary to point out that not all FEA software are using same parameter symbols. To avoid confusion in parameter definitions, it is always recommended to check model definition before apply model to simulation.

$\hat{S}$[MPa]	A[1/s]	Q/R[1/K]	m	n	a	ξ	h_0[MPa]	s_0[MPa]
27.11	69.53	5240	0.2598	0.0917	1.017	0.4	27595	14.75

Table 3.2: Table of *Anand* model parameters determined from Au-Sn creep shear test

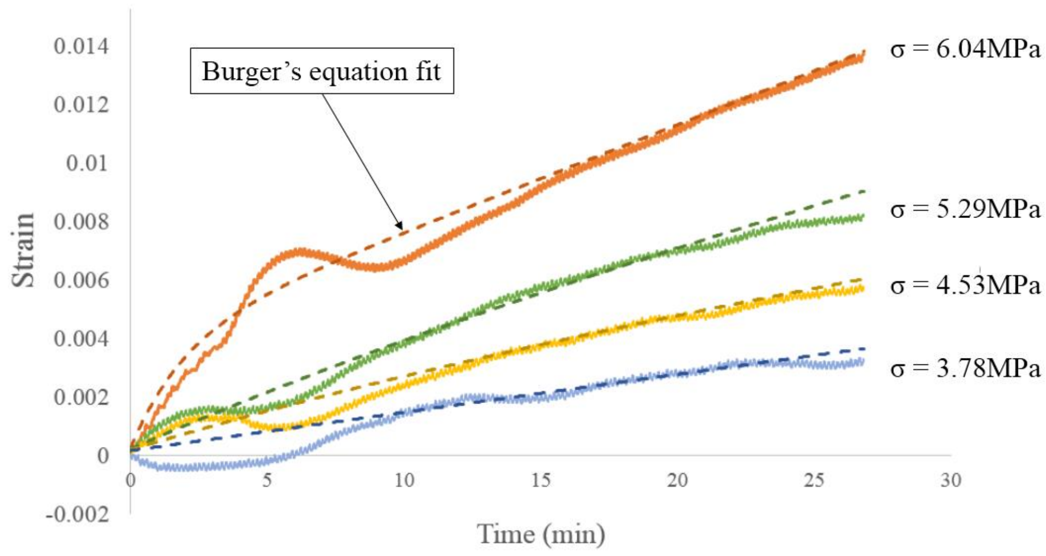

Figure 3.19: Strain versus time plots from experiment output and Burger's equation fit curves(T=175°C)

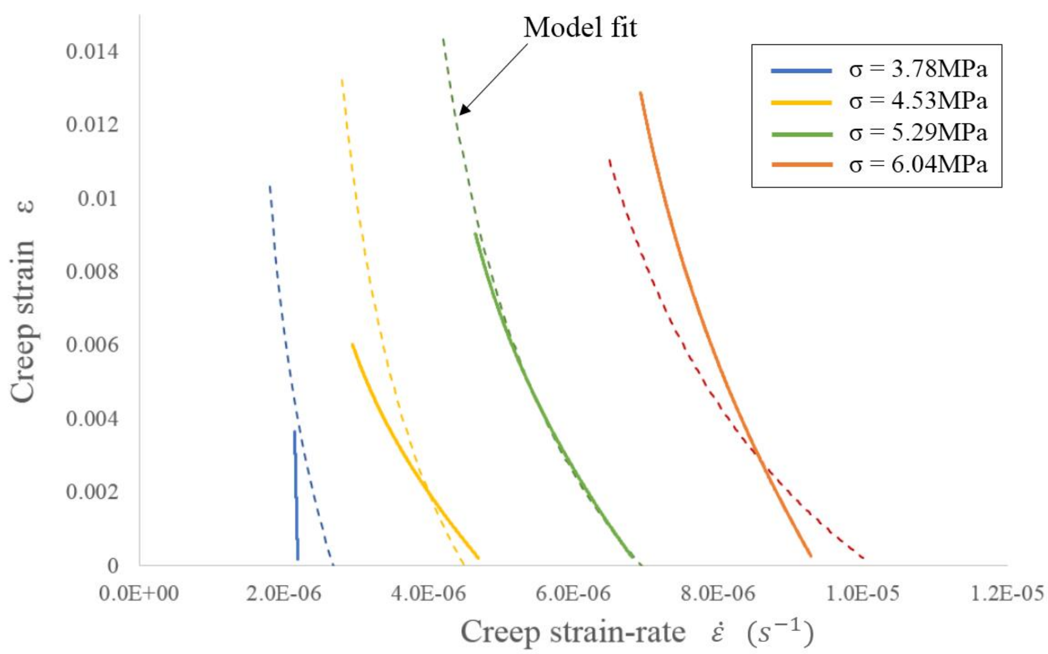

Figure 3.20: Strain versus strain-rate curve for parameter fit of Anand model(T=175°C

3.5.2. Model Validation

Since the parameters of *Anand* model have been determined by data fitting, it is necessary to validate the model by using it in a reconstruction of shear creep tests simulation, then compare the model prediction data with experiment data. A 2-D model of sample#58 was constructed in COMSOL Multiphysics 5.2 with mesh shown in Figure 3.21. Horizontal force is applied on a ideal rigid body that shear the Au-Sn solder joint. The joint has dimensions measured from Au-Sn joint of sample#58.

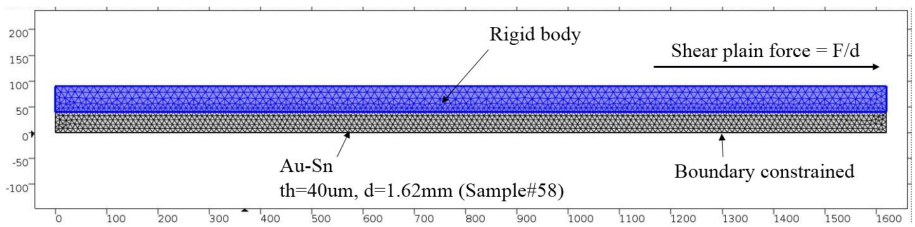

Figure 3.21: 2-D FEA model of the Au-Sn shear creep test sample

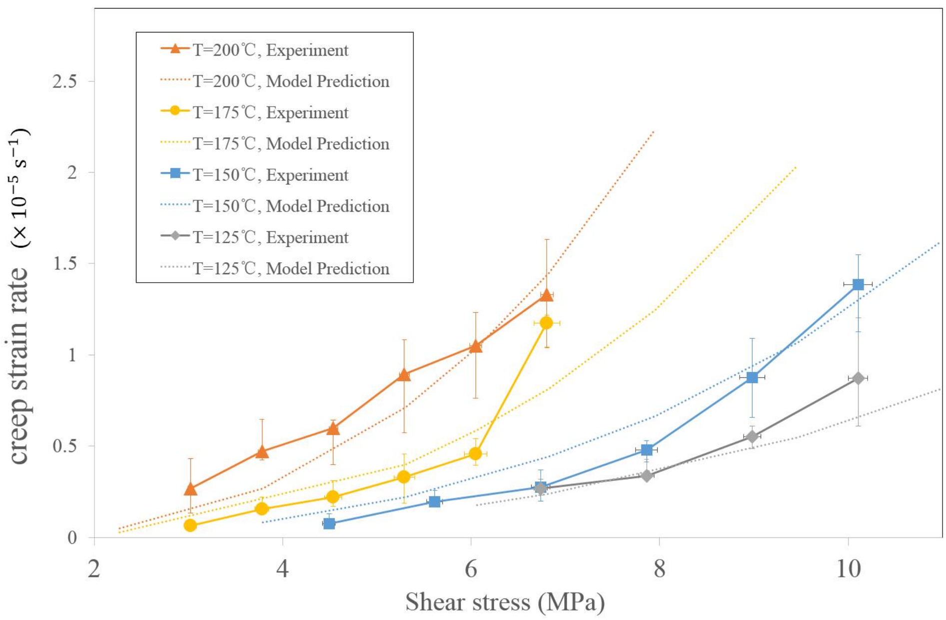

Figure 3.22: Validate Anand model parameters with steady-state creep strain-rate versus shear stress for Au-Sn

Same force loading profile as experiment was used in the simulation for a time-dependent study, and it was repeated with different shear stress and temperature settings. The compared steady-state creep strain rates versus shear stress curves are shown in Figure 3.22. Apart from several deviated data points, the steady-state creep strain rate from *Anand* model prediction agrees with experiment data.

4

Microstructure Effect on Viscoplastic Properties of Au-Sn Solder

In general definition, microstructure is the physical structure of material under observation of microscope. In many materials like metal(especially alloys), polymers and composites, microstructure can significantly influence macro-scale behaviors, such as thermal, chemical, mechanical properties, etc. Therefore microstructure study is one of the most essential discussions for material property study since it reveals most mechanical appearances with underlying mechanisms. In this chapter a qualitative investigation of microstructure effect on Au-Sn solder viscoplastic performance is conveyed by the established characterization method.

4.1. Introduction

Au-wt%20Sn composition consists of two major phases at solid state: ζ-phase(Au_5Sn) and δ-phase(AuSn)[39][40][41]. The microstructure of

Au-Sn solder alloy varies in phase type, phase distribution and phase conversion due to many factors such as reflow process and interface effect.

In reflow process, Au-Sn die-attach solder is heated with a programmed profile and attached to bond the die and package substrate. Many research reveals that the reflow profile is one of the key facts that determine the microstructure of Au-Sn solder interconnects, which can remarkably differ by changing key parameters in reflow temperature profile. Higher TAL temperature or lower ramp rate during liquidus phase is found to contribute to excessive large ζ-phase grains[42]. Same result is observed by using lower cooling rate, when conversely a fast cooling rate(>10K/sec) the large grains of ζ-phase start to be suppressed but small particles of δ-phase are expected to appear[43]. This study reveals the relationship between reflow cooling rate and microstructure after solidified, when a slow cooling profile with conventional air cooling processes results large dendrites of ζ-phase, while fast cooling rate by copper injection and copper suction suppresses large primary phase to generate and tends to result in uniform phase dispersion. The mechanism of this phenomenon is discussed in following section.

Studies[44][45] have been carried out about the interfacial effect of Au-Sn solder. Package substrates are often coated with Ni, Ti, Pt or Au to adjust interfacial behaviour. Extra intermetallic compounds is expected to form at the boundary between Au-Sn and substrate due to atom diffusion and electrical reaction, even void might be created [46]. The microstructure variation introduced by interfacial effect also depends on temperature which makes it more complex to analyze. In most cases pure gold(Au) coating is used to avoid extra metal components into Au-Sn system but still the microstructure near interface will be changed due to Au proportion difference that gold-rich phases will be very likely to group in to dominant phase near gold coating interface.

It is worth to investigate how the mechanical properties, especially viscoplastic properties of Au-Sn solder will be changed due to the microstructure variation, and so as how these changes will influence reliability performance. Despite of lot of similar studies being carried out on other widely used Pb-free materials such as SAC, surprisingly few studies of the mechanical properties with regard to microstructure effect on Au-Sn solder exist in literature. In the work of Namazu et al.[10], XRD tensile and creep tests were carried out to Au-Sn solder ball specimens, with the creep properties measured temperature ranging from 323K to 373K. The test was taken on eutectic Au-Sn specimen, properties of individual phases were not given. Liu et al.[26] studied thermal mechanical properties of the eutectic Au-Sn solder using nanoindentation, and the indentation mark was large enough to cover both ζ-phase and δ-phase grains so the measurement gave a global characterization of mixed phases instead of a fully portable element model on each phase. In the work of Chromik et al.[47], mechanical properties of the different Au-Sn phases were tested respectively, including elastic modulus, hardness and short-time creep behaviour. Quasi-static elastic and plastic properties of multiple intermetallics were measured using nanoindentation. The ζ-phase and δ-phase were found having higher hardness and stress, and comprising enhance the creep behaviour of the eutectic solder. However the experiment was taken only under room temperature. In the work of An et al.[48] the elastic and plastic constants of single-crystal ζ-phase and δ-phase were determined by ab initio calculations using psedopotential plane-wave method, however the values were not perfectly matched with experimental results. Conclusion can be made that many studies have been carried out for years about properties of Au-Sn solder, including viscoplastic properties. Several literature includes classic creep models trying to generally describe the viscoplastic behaviour under certain circumstances. However, there exists no fully experiment-based model of viscoplastic properties that takes microstructure effect into consider. From related studies of other solder materials, the microstructure is one of the most significant factor that determine the reliability properties of these solder joints, and so it might be for Au-Sn solders. The objective of this part of work, it to study how the viscoplastic properties of Au-Sn solder will change due to the microstructure variation, and so as how will the change influence reliability or lifetime predictions, where the viscoplastic properties characterization method established in Chapter 3 was used.

4.2. Change Au-Sn Microstructure by Controlling Reflow Cooling Rate

4.2.1. Sample Preparation

In this work, the method to change Au-Sn microstructure is controlling reflow cooling rate, which has been generally investigated in many other materials. The sample design with flanges and Au-Sn preforms is identical as stated in the Chapter 3, and preparation procedures are very similar. The only controlled parameter is reflow profile, specifically cooling rate. In previous work the specimens were prepared with standard reflow profile, which has rapid cooling rate(RC) of 4K/sec. Literature[43] indicates that to obtain remarkable difference in microstructure, the cooling rate between test groups should be very large. Therefore, slow cooling rate(SC) of 0.2K/sec and fast cooling rate(FC) of 200K/sec are adopted in following experiments. Including RC specimens in previous chapter, there are three reflow profiles(Table 4.1 in total to be investigated.

Reflow profiles	Cooling rate	TAL time	Cooling method
Slow cooling rate (SC)	0.2K/sec	238.3 sec	Reflow oven
Rapid cooling rate (RC)	4K/sec	48.3 sec	Reflow oven
Fast cooling rate (FC)	200K/sec	38.5 sec	Water cooling

Figure 4.1: Parameters of three reflow profiles

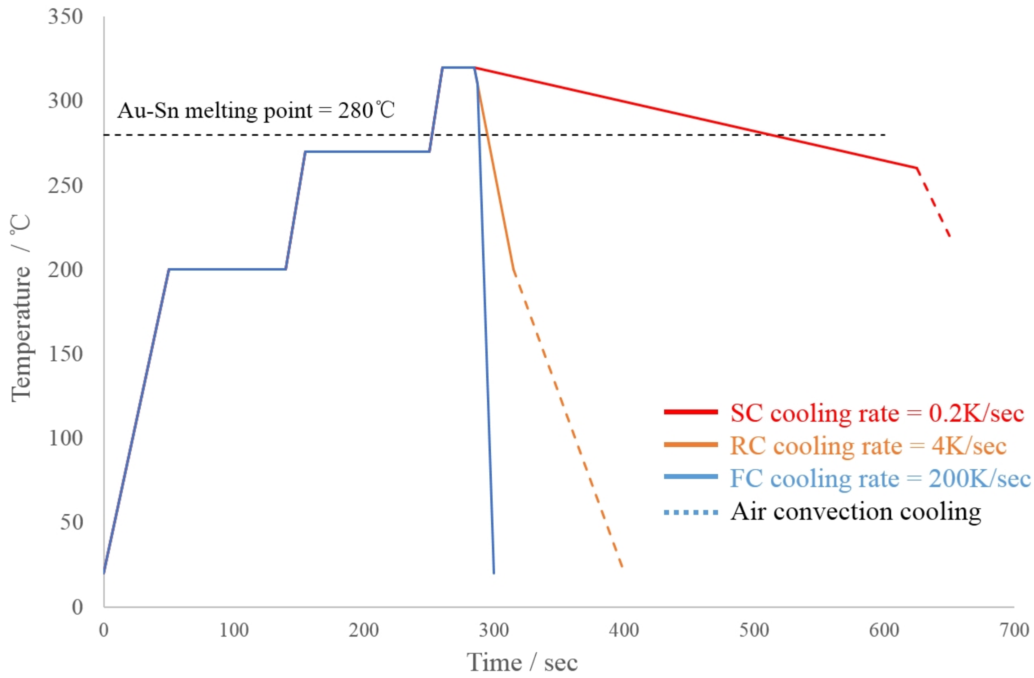

Figure 4.2: Three reflow profiles with different cooling rates

Figure 4.2 presents three reflow profiles for potentially leading to different Au-Sn microstructures. Three profiles are identical in gas configurations, i.e. the profile for vacuum and mixed gas of hydrogen and nitrogen will be identical for all profiles. Temperature controlling in all profiles have identical heating program, too. After TAL phase, both SC and RC cooling rates were controlled by reflow oven when they are still in range of reflow oven's temperature controlling capability, yet it could not provide higher cooling rate to achieve FC cooling rate of 200K/sec. Therefore FC profile specimens were immediately taken out from reflow oven to a water container, where water cooling method is able to fast cool the whole set-up from 320°C down to room temperature less than 1.5 seconds. It is noticeable that during TAL phase the oven chamber was charged with mixed gas of hydrogen and nitrogen, therefore for safety reasons, pure nitrogen gas was quickly charged before taking out specimens to flush risky hydrogen out of chamber. Even safety action might slightly influence fast cooling rate because the specimens might be slightly cooled down by flushing nitrogen gas before taken out from chamber, the flushing action happened extremely fast that the Au-Sn would still in melting state before taken into water cooling, and the cooling rate was dominated by water cooling during Au-Sn solidification.

4.2.2. Microstructure Investigation

Scanning electron microscope(SEM) imaging is a necessity to examine microstructure of An-Sn die-attach layer after reflow process. In this work, cross-section SEM samples were made for energy filtered back scattering electron(BSE) imaging, which were prepared in standard cross-section SEM sample procedures:

1. Stabilized the soldered flanges by gluing two $2mm$ brass rods in the align holes
2. Smear additional epoxy around the specimen
3. Mark Au-Sn soldered area by optical microscope
4. Saw the epoxy stabilized specimen at soldered area
5. Grind and polish cross-section surface with $3\mu m$ Mylar bonded diamond films on a glass plate
6. Polish using cloth sequentially from $3\mu m$, $1\mu m$, $0.25\mu m$ to $0.1\mu m$ diamond slurry
7. Polish using $60nm$ colloidal alumina with propylene glycol as coolant to highlight the microstructure

The prepared cross-section specimen ready for SEM imaging is shown in Figure 4.3, and BSE SEM images of three types of specimens are shown from Figure 4.4 to 4.6.

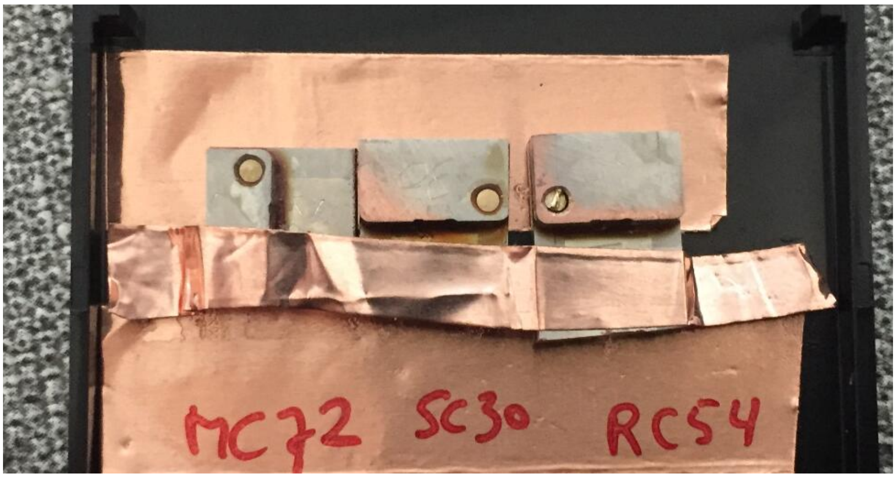

Figure 4.3: Cross-section specimens for SEM imaging

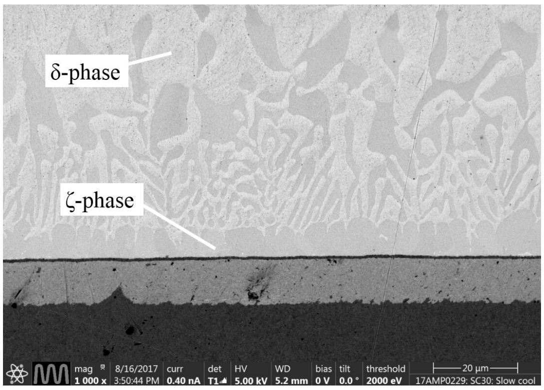

(a) 1000X

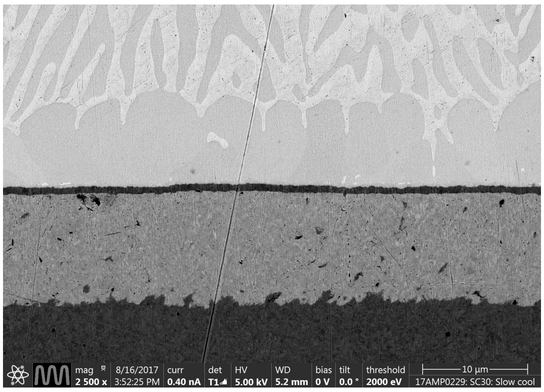

(b) 2500X

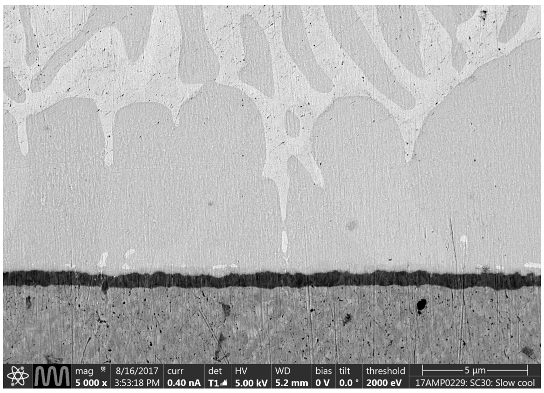

(c) 5000X

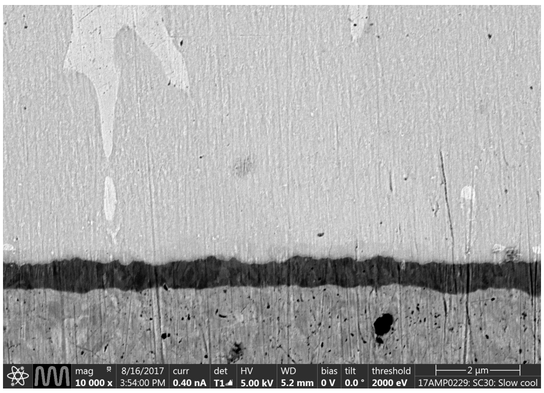

(d) 10000X

Figure 4.4: BSE images of Au-Sn microstructure with slow cooling rate(SC)

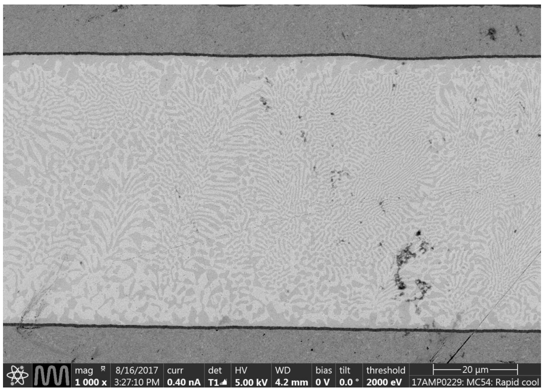

(a) 1000X

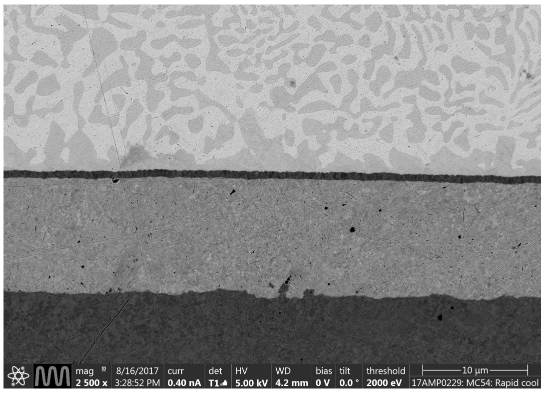

(b) 2500X

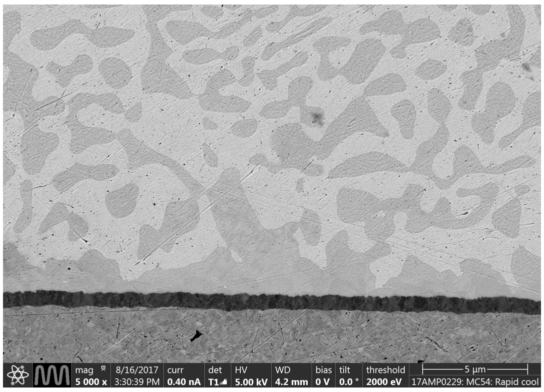

(c) 5000X

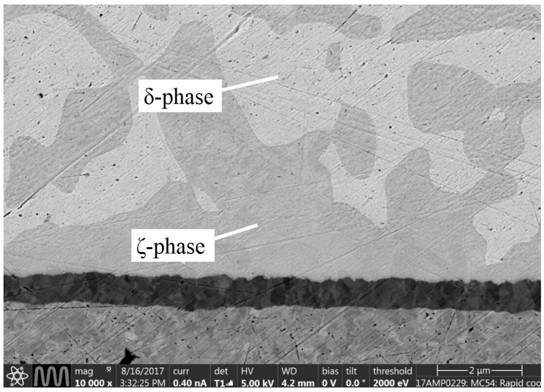

(d) 10000X

Figure 4.5: BSE images of Au-Sn microstructure with rapid cooling rate(RC)

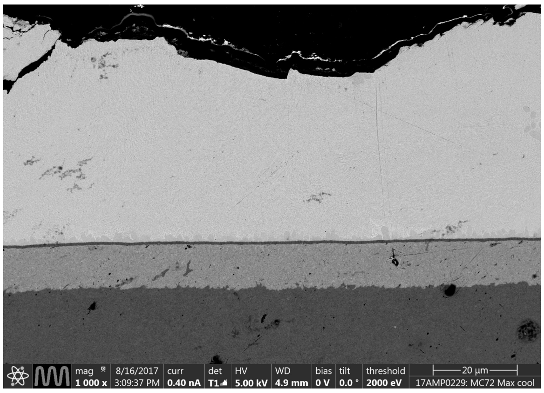

(a) 1000X

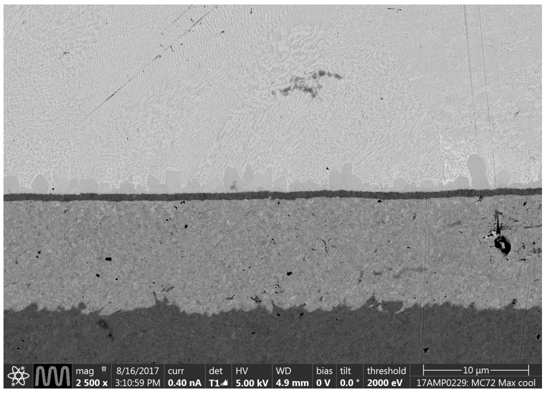

(b) 2500X

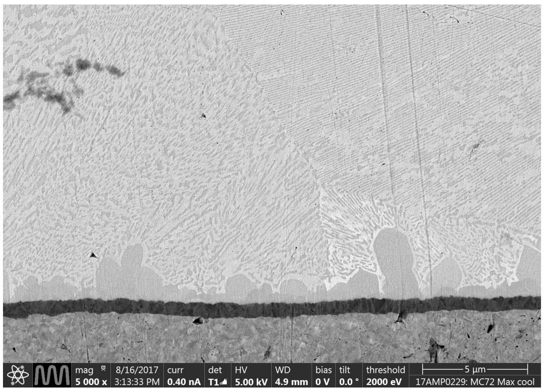

(c) 5000X

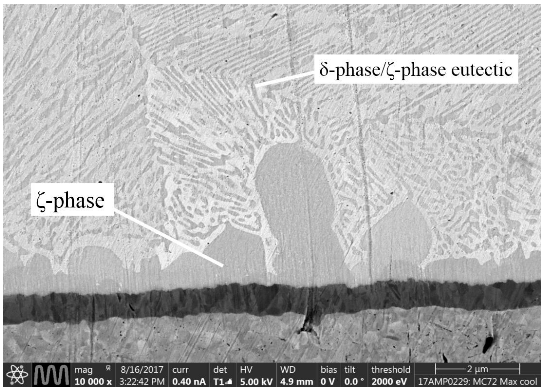

(d) 10000X

Figure 4.6: SEM BSE images of Au-Sn microstructure with fast cooling rate(FC)

Reflow profiles	SC	RC	FC
Cooling rate	0.2K/sec	4K/sec	200K/sec
Phase	δ-phase/ξ-phase	δ-phase/ξ-phase	δ-phase/ξ-phase
Phase distribution	Coarse dendrite matrix	Fine matrix	Fine eutectic
Phase size	>2um	~1um	<0.2um
Interface phase	δ-phase bumps thickness~5um	δ-phase bumps thickness~1um	δ-phase bumps thickness~0.8um

Figure 4.7: Microstructure features of Au-Sn in three reflow profiles

For the most simple case, only the two major phases in Au-Sn solder: ζ-phase and δ-phase are considered. Identical feature for all three types of specimens was found that these two major phases dominate entire cross-section. This can be explained from the phase diagram of Au-Sn alloy system(Figure 4.9). As stated previously, Au(80wt%)-Sn(20wt%) composition is widely adopt as solder alloy for the reason that this eutectic is formed at phase transition point between two steep liquidus lines to provide favourable soldering and bonding performance, and so as the Au-Sn preforms used in this work. Ideally the whole Au-Sn preform melts at 280°C, becomes liquid in reflow TAL phase, and re-solidifies at 280°C, and forms eutectic composition when cools down. The composition should have Au:Sn atom fraction of 2.5:1, however there is no such phase exists in Au-Sn crystal system. Therefore in reality a ζ'-phase is formed, which is in fact a mixture of two phases: ζ-phase(atom ratio Au:Sn=5) and δ-phase(atom ratio Au:Sn=1). It also explains volume ratio of two phases should theoretically be 3:5 to combine a total Au:Sn atom fraction of 2.5:1 when no foreign atoms are brought into the system. It is necessary to point out that during SEM imaging no elemental analysis or chemical characterization methods were taken, such as Energy Dispersive X-ray spectroscopy(EDX) to identify phases. The following work based on identifying phases in images are based on referring to similar images in existing study.

Remarkable microstructure differences are found from SEM images between three types of specimens treated with different reflow profiles, mainly expressed in two regions: dominant phase region and interfacial phase region. The two features locate in different areas of Au-Sn(Figure 4.8).

Dominant region phase morphology refers to the microstructure feature near centered area of Au-Sn solder, where bonding interfaces are too far to influence Au-Sn microstructure. A standard reflow profile with RC cooling rate results a fine matrix distribution where both ζ-phase and δ-

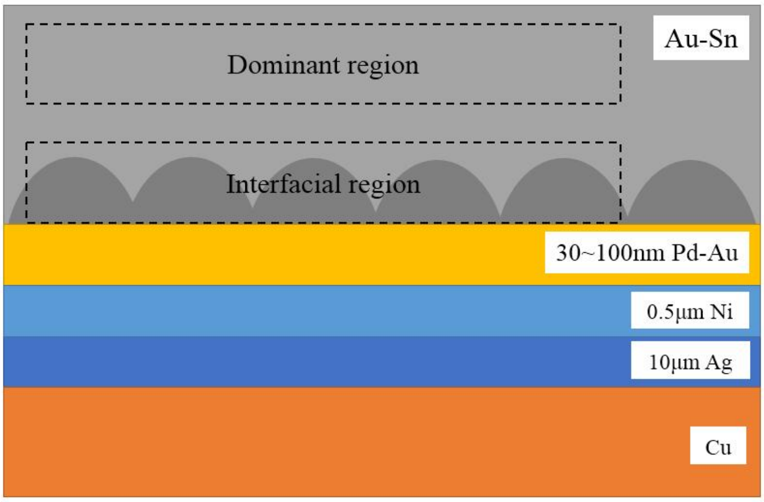

Figure 4.8: Two main microstructure morphology regions

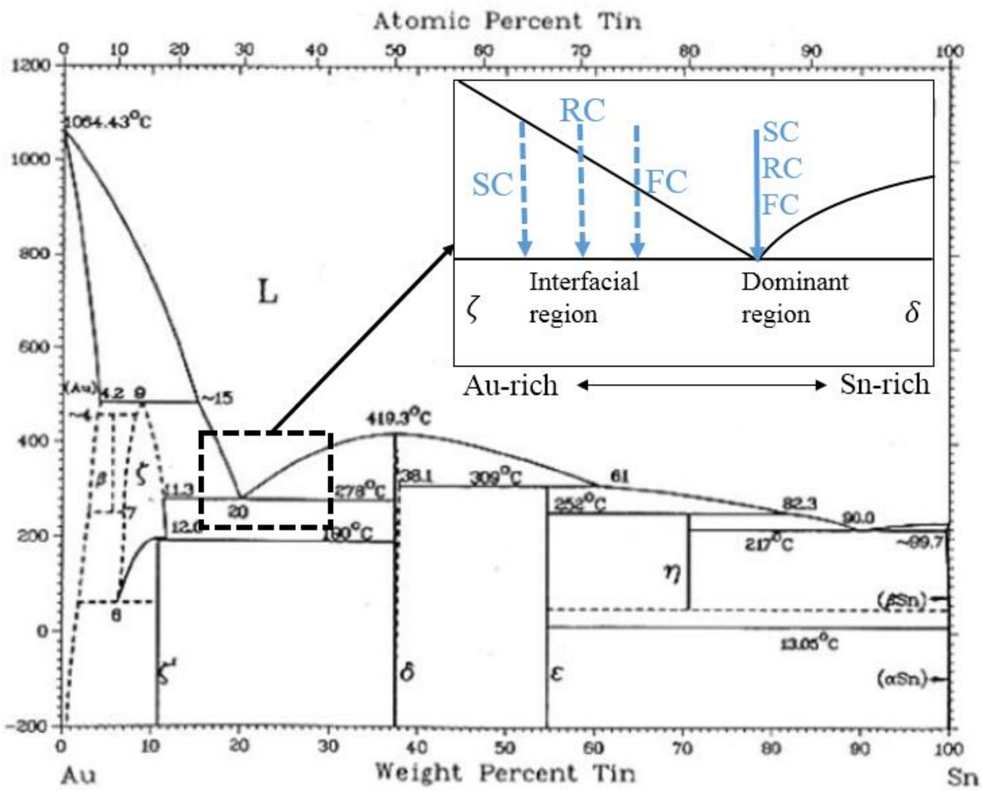

Figure 4.9: Phase diagram of binary Au-Sn systems [5] and different solidification paths near interface

phase are uniformly dispersed into polygonal particles with around $1\mu m$ size. White δ-phase shows more continuity than dark ζ-phase islands since the former has higher proportion. Compare to standard RC profile, the slower cooling rate SC profile results a very different coarse dendrite matrix morphology, where long dendrites of two phases appear with coarse mono-phase areas. Most dendrites lay in the direction perpendicularly to the interfacial boundary. The last reflow profile shows contrary results that the extremely fast water cooling leads to a fine semi-eutectic and highly uniform phase distribution, where both two major phases are restrained into very fine size less than $0.2\mu m$. The mechanism of morphology difference against cooling rates can be explained from phase nucleation rate. Both ζ-phase and δ-phase are formed by nucleation at the steep phase lines at melting point, and nucleation rate is limited by atom diffusion. At slower cooling rate(i.e. SC profile) the long solidification duration allows longer nucleation process under high temperature, where more atom diffusion results larger dendrite phases. On the contrary at higher cooling rate(i.e. FC profile) the solidification temperature has a instant drop that even supercooling in Au-Sn occurs. The phase nucleation duration is significantly suppressed by limited atom diffusion time, and results an eutectic microstructure. Similar phenomenon that a fast cooling rate results a finer dispersion of microstructure has been found in multiple solder alloys [49][50][11][51][52].

Interfacial region phase morphology refers to the microstructure feature near bonding interfaces where external materials can influence Au-Sn microstructure. All three reflow profiles result an dominant phase layer near interface, which is formed by ζ-phase bumps as shown in Figure 4.8. However different in cooling rates leads to variation on thickness of interfacial phase layer, when SC profile results large ζ-phase bumps that thickness of interfacial layer goes over $5\mu m$ at most places, while RC and FC profiles have similar interfacial phase morphology that the ζ-phase layer thickness is around $1\mu m$. The mechanism of ζ-phase layer forming at interface is explained with Au-Sn phase diagram. The bonding surface of flanges has Pd-Au coating, which provides a gold-rich environment at interface. External Au atoms migrate into Au-Sn solder because of atom diffusion accelerated by high temperature during reflow [53], and change the solidification path. Au atom migration shifts the composition of Au-Sn system to less Sn percent(solidification path shifts left in Figure 4.9), resulting a gold-rich ζ-phase enrichment near interface. Due to slow cooling rate in SC profile, the TAL time is much longer than RC and FC profiles, in which case the ζ-phase enrichment lasts longer in high temperature, leading to thicker ζ-phase layer near interface.

4.3. Shear Creep Experiment

Same shear creep experiment in chapter 3 was taken with Au-Sn specimens produced with SC and FC profiles. Design of experiment and result shown in Figure 4.10, 37 groups of shear creep data were recorded out of total 47 tests. Some test combinations of load force and temperature were skipped for experiment simplification. The FC samples suffered too short period of solidification that the microstructure might be changed due to thermal annealing effect. To avoid irrelevant exposure of high temperature condition, the hold-and-creep time for FC shear tests were limited in 15 minutes.

Challenges were found during Au-Sn joint area measurement. In previous experiment on RC samples, the majority of soldered joints kept in one solidified piece with barely consistent area. In this part of experiment, the SC samples were treated with longer TAL time, which means the Au-Sn solder had longer duration in liquid state, and tended to form a circular joint area, but still has consistency in area measurement. However during the preparation of FC samples, the set-ups were directly moved out of reflow oven when Au-Sn was still in liquid state, and cooled by immersing into cold water, which created violent vibration of

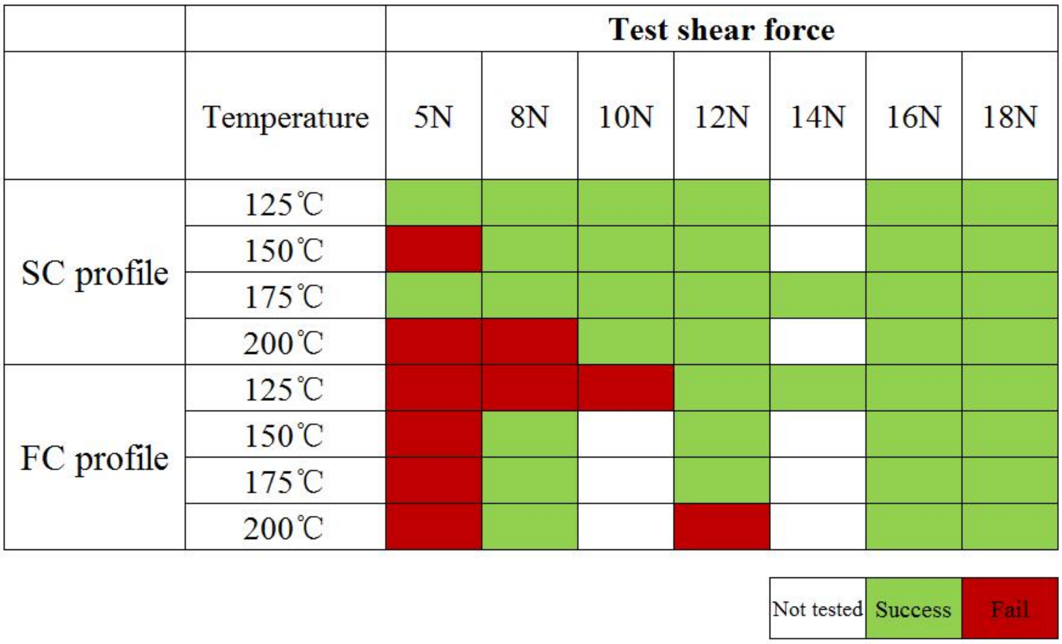

Figure 4.10: Design of experiment for shear creep tests

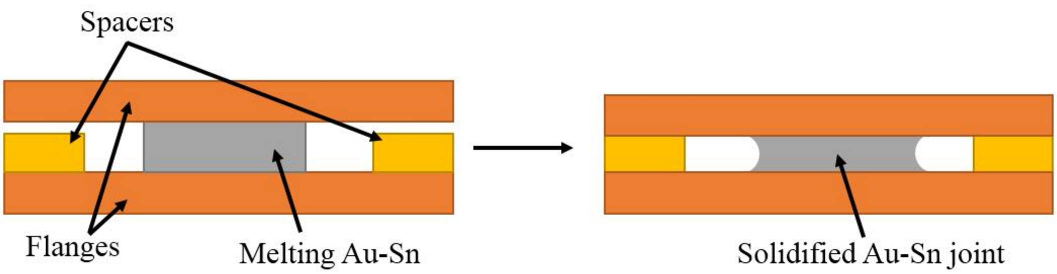

(a) SC and RC samples

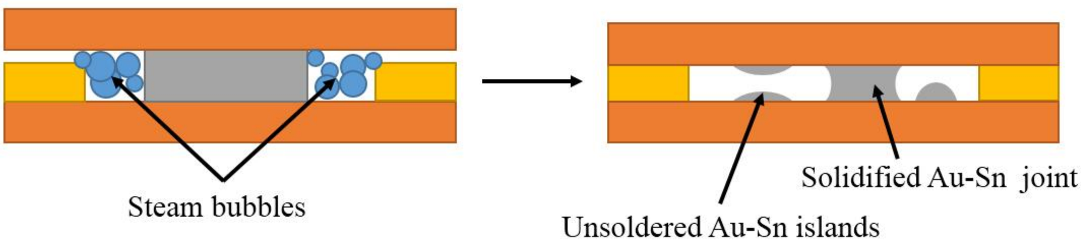

(b) FC samples

Figure 4.11: Au-Sn joint shape inconsistency because of cooling methods

seething boiling water. Furthermore, the hot set-ups first boiled water at surface, creating steam bubbles around Au-Sn joints. Impacted and squeezed by vibration flanges and bubbles, the Au-Sn joints were solidified into irregular shapes, or even pushed out forming non-soldered islands(Figure 4.11(b)), which eventually produced large inconsistency in measuring joint area in FC samples. Most FC samples have smaller joint area than SC, RC samples, which means they were applied higher shear stress under same load force.

Steady-state creep strain-rate is used as a key indicator in comparing different reflow profiles, or as explained in previous section of this chapter, comparing different Au-Sn microstructures. The comparison of four temperature conditions is shown in Figure 4.12. Separation of steady-state creep strain-rate is observed in all tested temperature conditions that at same shear stress the SC samples have higher creep strain-rate, the standard RC samples come the second, and the FC samples have better creep resistance. Similar phenomenon that the steady state creep rate is suppressed when the phase particles in solder microstructure is refined in many solder alloys[54][55][56][57]. Hypothesis was proposed on basis of creep mechanisms of dislocation climb and grain boundary sliding. The dislocation climb requires larger particles that provide unstable sharp transition between particles, where a finer dispersion of phase particles becomes resistance force on dislocation. On the country side, larger interfacial regions between two phase regions provide more probability of grain boundary sliding. In this case, creep is easier to be triggered in microstructure that has coarsened dispersion of phase regions such as FC samples, where dislocation climb and grain boundary slide are both enhanced.

Viscoplastic models of Au-Sn solder with SC and FC profile were also built from experiment data, with same fitting method described in chapter 3. Table 4.1 lists parameters of *Anand* viscoplastic models for both two types of Au-Sn solders. Following Figure 4.13 depicts the validation of model predictions with experimental data of SC an FC profiles. Identical validation method including FEA model and mesh was used.

	$\hat{S}$[MPa]	A[1/s]	Q/R[1/K]	m	n	a	ξ	h_0[MPa]	s_0[MPa]
SC	82.18	250.5	5965	0.3380	0.0900	1.200	0.5	2162.1	15.61
FC	28.92	403.6	5187	0.1597	0.00913	1.336	0.5	398.28	19.37

Table 4.1: Anand model parameters for SC and FC profiles

4.4. Reliability Simulation Based on Au-Sn Viscoplastic Models

The viscoplastic model of three types of Au-Sn die-attach solders with different microstructures controlled by reflow profiles were obtained so far. In order to find out how microstructure difference would influence the reliability performance of devices that uses Au-Sn as die-attach solder, temperature cycling simulations were performed by FEA method, while viscoplastic models were used to predict creep strain energy density in a typical structure of die-attach device. Figure 4.14 shows the simulated 2-D model of a typical die-attach structure, in which the material properties of silicon die and copper substrate are adopted from built-in library, and other parameters except viscoplastic models were adopted from existing literature[47][58].

It is reported that the accumulation of creep strain energy density in each thermal cycle becomes stable after 3 cycles[59], there for only 4 cycles were applied in simulation, which was sufficient for qualitative comparison among three microstructures. Figure 4.15 shows the temperature cycling profile used for FEA simulation.

To describe solder reliability performance corresponding to mechanical properties, the energy based fatigue model theory[60] was referred in this work, which gives a theory of predict solder fatigue possibility on basis of accumulation of strain energy density. In the original the-

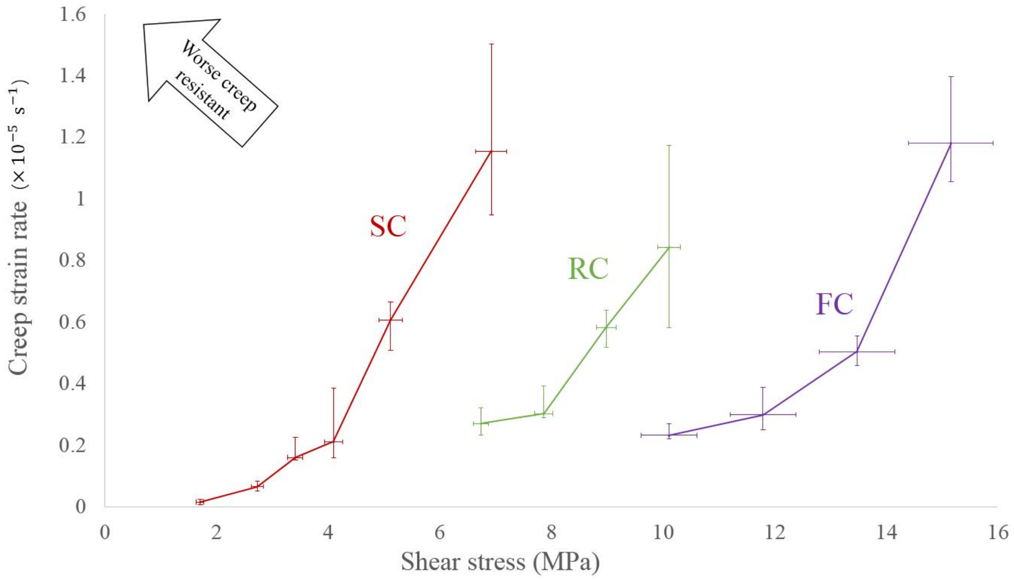

(a) T=125°C

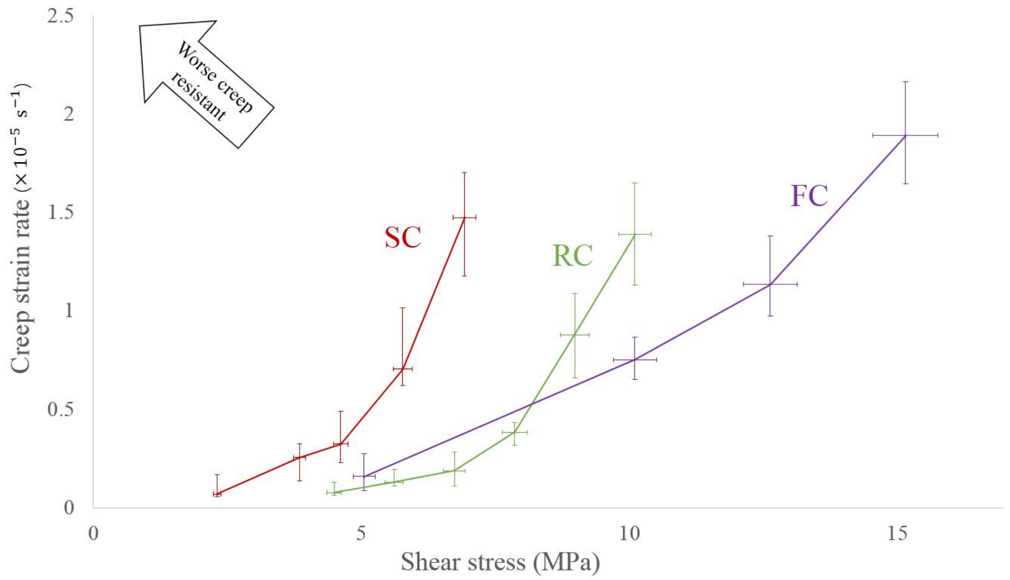

(b) T=150°C

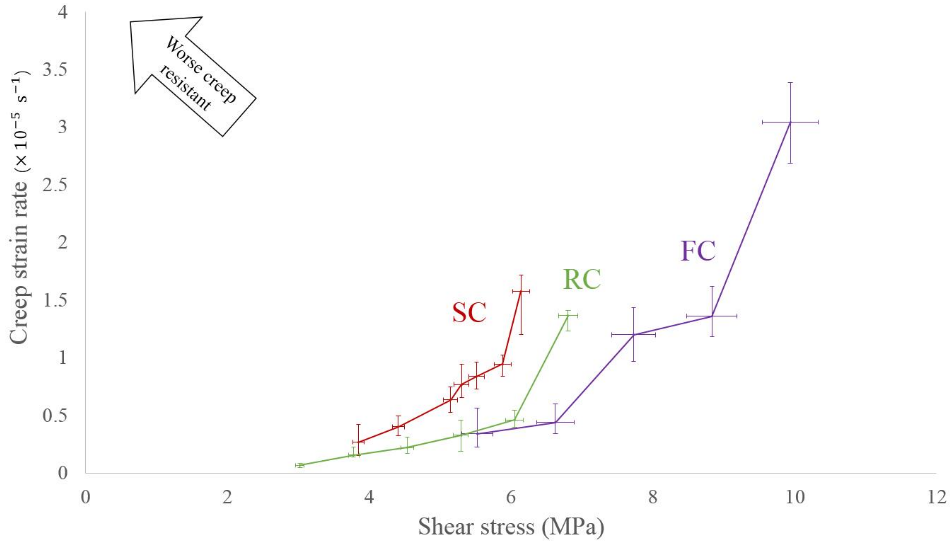

(c) T=175°C

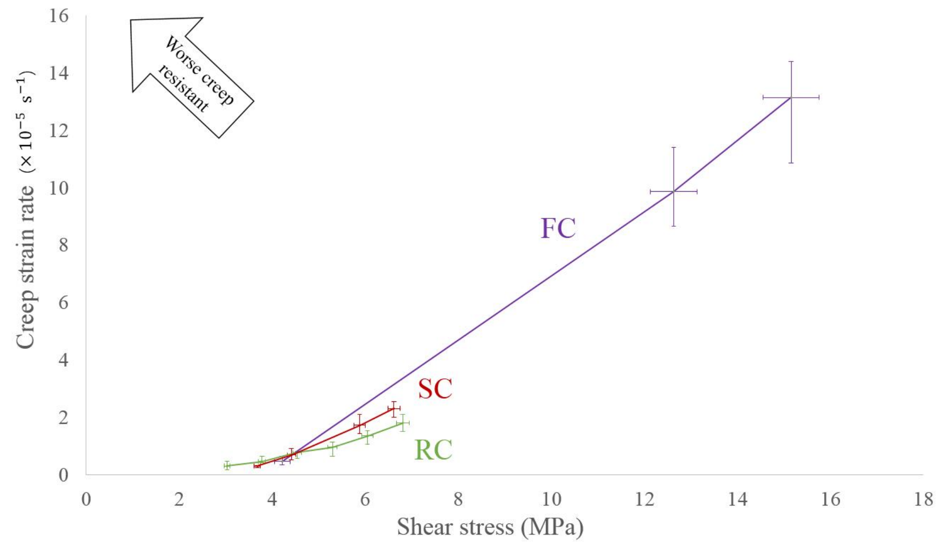

(d) T=200°C

Figure 4.12: Creep strain-rate versus shear stress in different temperature

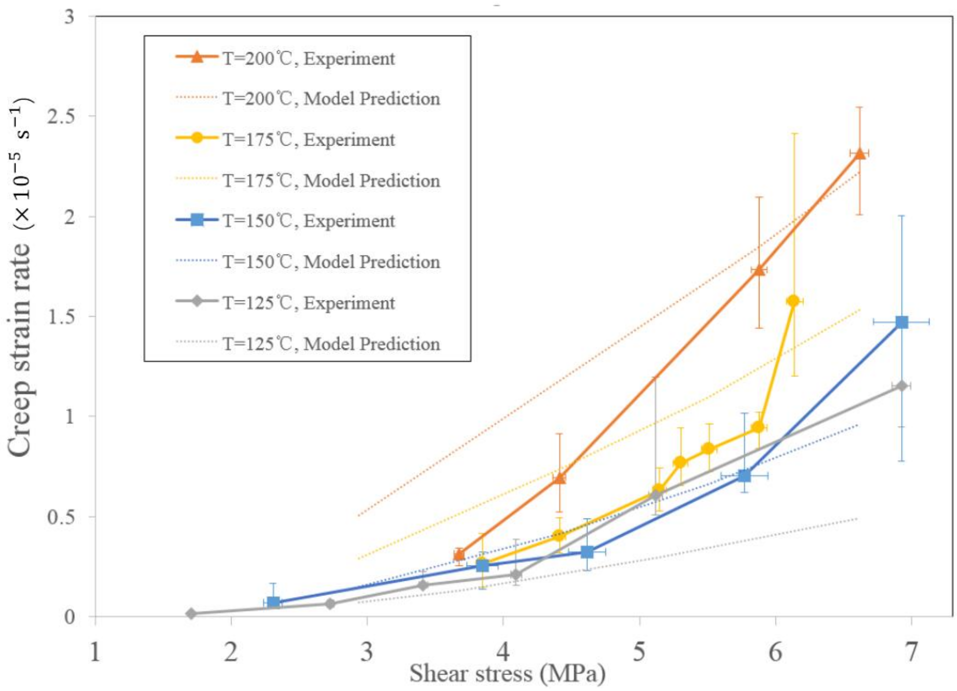

(a) SC

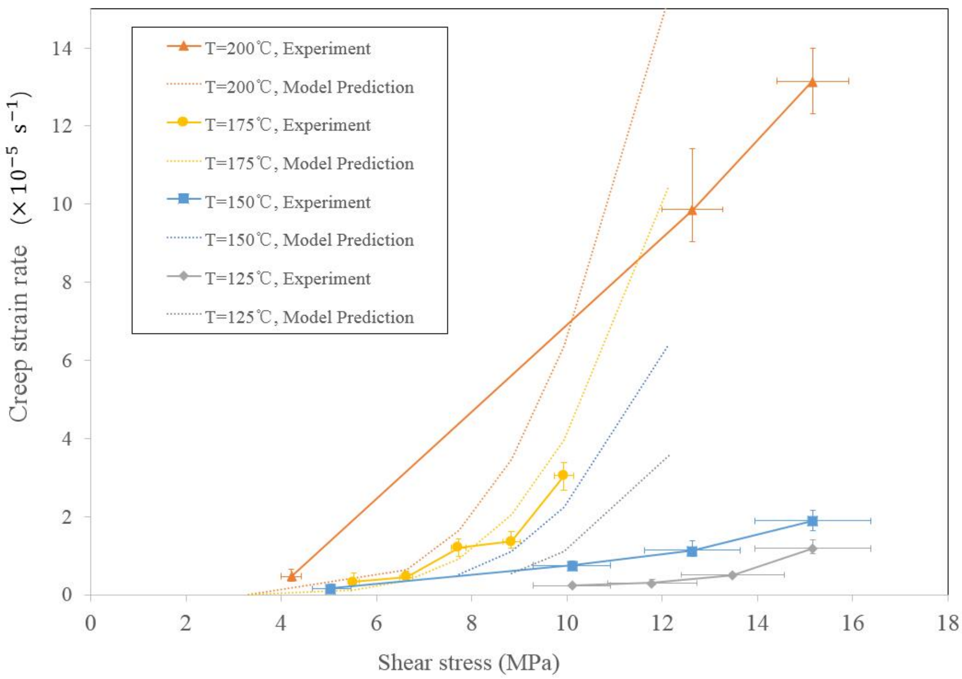

(b) FC

Figure 4.13: Validation of Anand model parameters with steady-state creep strain-rate versus shear stress for Au-Sn

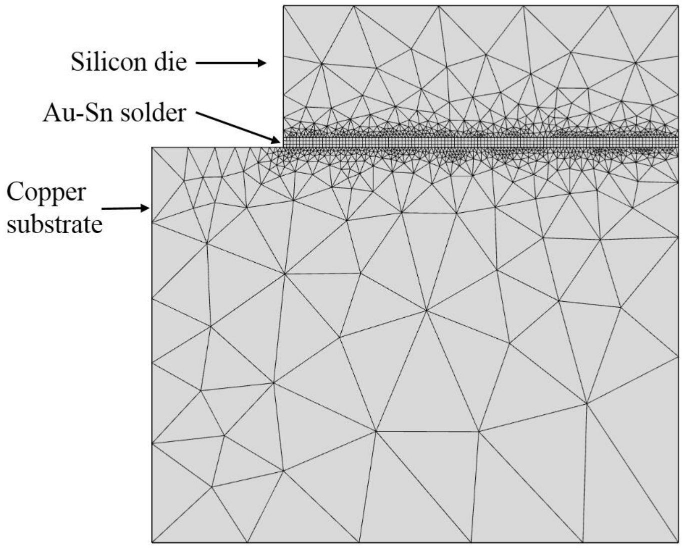

	Length	Width	Thickness
Silicon die	1.20mm	0.50mm	200um
Au-Sn solder	1.20mm	0.50mm	15um
Copper substrate	1.60mm	0.50mm	600um

Figure 4.14: Die-attach structure model and mesh in simulation

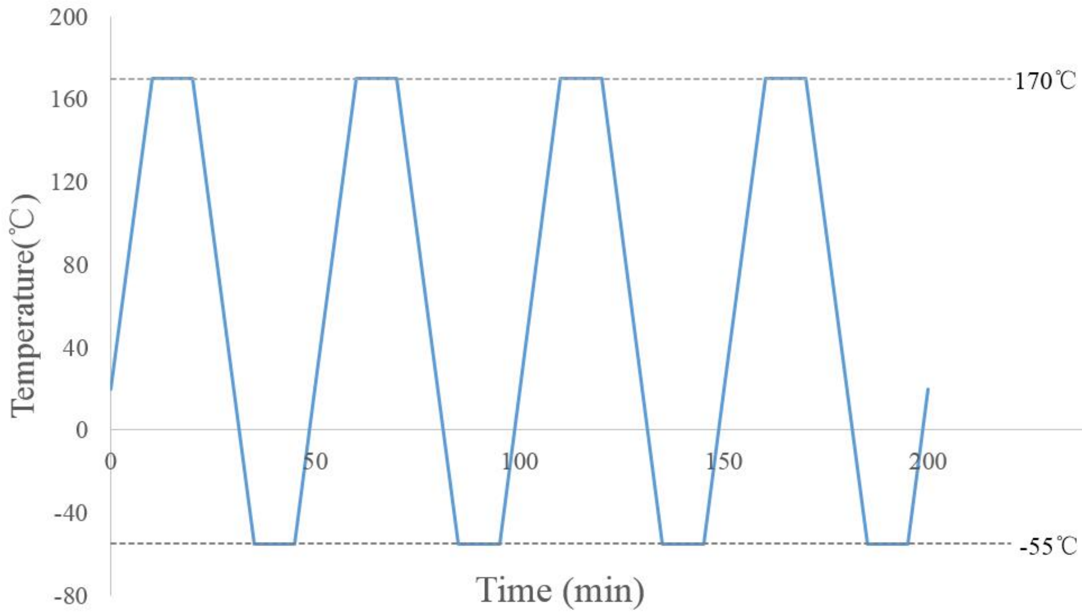

Figure 4.15: Temperature cycling profile used for FEA reliability simulation

ory three aspects of strain energy density generated by elastic strain, rate-independent strain and viscoplastic strain, and the first two were ignored in following simulations since investigation on viscoplastic strain is requested. The total strain energy density accumulation in each temperature cycle is expressed as Equation 4.1.

$$\Delta W = \Delta W_{vp} = W_{4th} - W_{3th} \tag{4.1}$$

where ΔW_{vp} is the viscoplastic strain energy density accumulation and is calculated as the creep strain energy density difference between the end of fourth and third cycle. Then the relationship between fatigue prediction and energy accumulation was proposed[61] in Equation 4.2.

$$N_f = (\frac{W_0}{\Delta W})^k \tag{4.2}$$

where N_f is the predicted lifetime, or number of cycles before failure during temperature cycling test. W_0 and $k(k < 1)$ are parameters for model correction. The model indicates that a faster strain energy density accumulation in temperature cycle is expected to result decrease in predicted lifetime, i.e. an earlier failure. The simulation in all cases clearly shows a high creep strain energy density accumulated region near edge of the Au-Sn solder die-attach layer(Figure 4.16), where is expected to be the most critical region that has very high possibility to have early crack during device lifetime. Most elements near center of Au-Sn solder has very low creep strain energy density which means these regions are less relevant to device fatigue caused by creep strain.

It is necessary to set a certain creep strain energy density threshold to separate critical region and non-critical region. Figure 4.17 shows the accumulated creep strain energy density distribution among all Au-Sn solder elements. It shows that all plots has a deviation point near 90% of elements, where the rest elements have much higher accumulated creep strain energy density. In this case, assumption is made that the elements after the deviation point, or so called critical point, are consid-

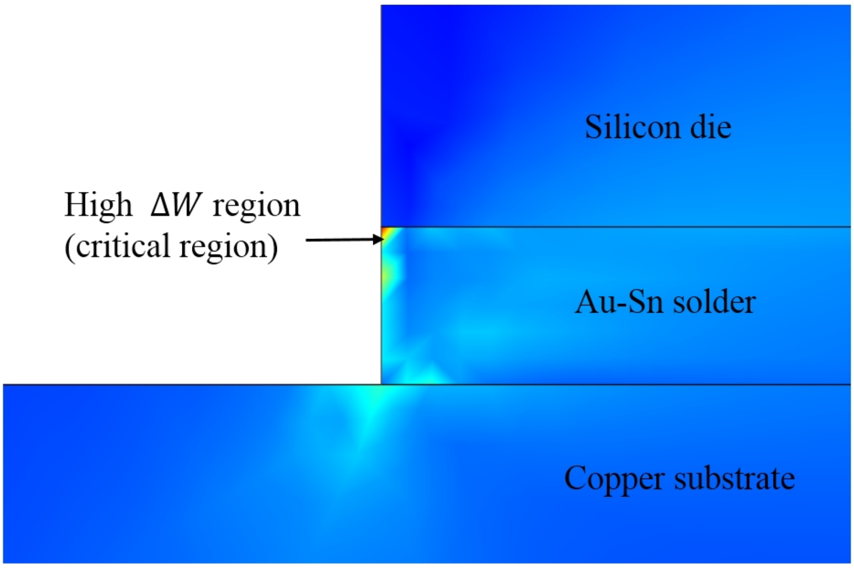

Figure 4.16: High creep train energy density accumulation region

ered as critical elements, and are very likely to be responsible for failure due to high strain energy density accumulation.

Simulation data implies that the both largest creep strain energy density accumulation and percentage of critical elements occur when SC model is adopted, the FC model results a lowest creep strain energy accumulation and critical area, and standard RC model between the two. According to the energy based fatigue theory, fast accumulation of creep strain energy accumulation results a decrease in predicted lifetime on basis of Equation 4.2. Therefore the predicted lifetime of three viscoplastic models are

$$N_{fSC} < N_{fRC} < N_{fFC}$$

The simulation result implies that the Au-Sn solder with FC reflow profile, in other words higher cooling rate during reflow process, will finally lead to a less creep strain energy accumulation, and a increase of lifetime, compared to standard RC reflow profile. On the contrary, SC reflow profile, or slower cooling rate for Au-Sn solder will result to a decrease in lifetime, or is more probable to have early fatigue during

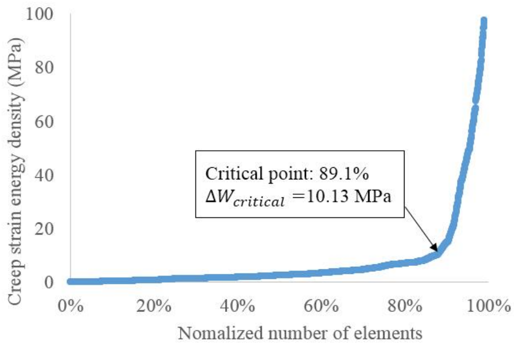

(a) SC

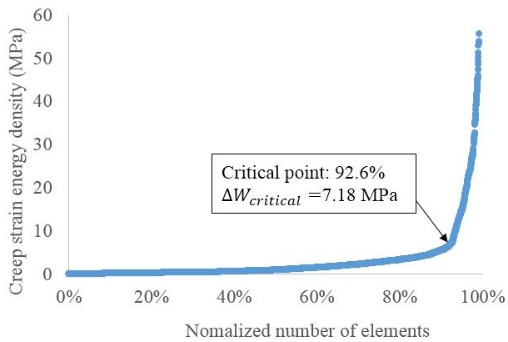

(b) RC

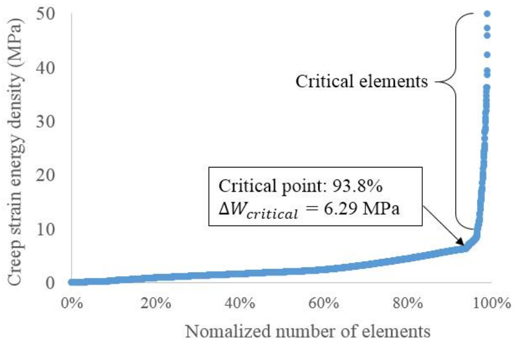

(c) FC

Figure 4.17: Accumulated creep strain energy density distribution among all Au-Sn solder elements and critical points

temperature cycling test.

It is important that simulations introduced in this chapter are nothing but qualitative comparison among three viscoplastic models, and cannot represent actual lifetime prediction since other material parameters such as elastic modulus or coefficient of thermal expansion are considered identical for all models, which should differ in reality. More material parameters are required for complete lifetime prediction.

5

Conclusions

In this work, an investigation on viscoplastic properties of Au-Sn die-attach solder was presented. A reliable method for Au-Sn solder viscoplastic properties characterization and quantified modelling was established by analyzing data from a series of mechanical experiments. A consistent experimental method to authentically observe and accurately measure the viscoplastic behaviour of Au-Sn solder was explained in detail. A well designed test set-up consists of flanges and Au-Sn preforms were fabricated with a certain sequence of procedures. A series of shear creep tests were then operated by DMA controlled conditions of multiple temperature and force, giving data groups that finally help to fitting for viscoplastic models. Viscoplastic properties of Au-Sn solder under tested conditions were described by a set of Anand model parameters that could directly adopted in FEA reliability assessment.

Furthermore, an investigation of microstructure effect on Au-Sn solder viscoplastic properties follows foregoing studies was presented. A consistent method to control Au-Sn solder microstructure was developed that by tuning reflow profile, specifically reflow cooling rate, the solidified Au-Sn die-attach joint is able to have different microstructure. Different cooling rate influences both dominant phase morphology and interfacial phase morphology and the phenomenon was explained by solidification path and nucleation theory. Similar shear creep tests wear applied on Au-Sn samples with three microstructures based on established method in previous studies. Reliability assessment was then taken and simulation results indicated that faster cooling rate results better creep resistance, and is expected to have increased lifetime during temperature cycling tests.

For fundamental material properties research, this study provides a complete methodology of viscoplastic properties characterization for Au-Sn solders, including experimental procedures and theoretical analysis. This methodology can be also ported to other materials including but not limited to new generation of Pb-free solder materials.

For industry applications, this study provides practical viscoplastic models of Au-Sn solder to be adopted to an accurate reliability assessments, and suggestions to potentially enhance Au-Sn solder reliability by optimizing microstructure corresponding to reflow cooling rate.

6

Suggestions for Future Works

This work still have limitations and faultiness needs to be clarify, and it can only be viewed as the beginning of fundamental studies on Au-Sn solder. Many new areas can yet be explored in future works. Some suggestions are presented as following.

Improve solder joint shape controlling
In present work, the Au-Sn preform shape was not restrained and resulted irregular joint shape after reflow process. Uncertainty on joint shape added extra work measuring joint area, and inevitably brought inconsistency of experiments. Furthermore, the variation of joint area also shifted shear stress away from desired testing range, potentially introducing extra mechanical deformation into pure creep tests, and making model fitting more complex. Improving method would be done in specimen preparation, that restricts the solder joints in a regular geometry such as rectangle. Additionally, true stress is then able to be used in calculations with benefits from regular joint shape. Potential designs are suggested: machine trenches or fences around preform to restrain melting solder in a certain area; or pattern protect layer like photo-resistant

to prevent melting solder flowing out. This will help to simplify experiment steps and increase sample consistency.

Add phase analysis method to microstructure investigation

In present work, identification of ζ-phase and δ-phase in SEM images are based on referring to similar images in existing study, which may not be correct due to variation of cross-section specimen preparation procedures. It is suggested that during SEM imaging, elemental analysis or chemical characterization methods should be taken, such as Energy Dispersive X-ray spectroscopy(EDX), to identify phases. Additionally, SEM imaging of Au-Sn samples before and after creep tests are suggested, to guarantee the microstructure not being changed due to creep test conditions, and help investigate creep mechanism. These are not for improving imaging quality or test accuracy, but for completeness of the microstructure investigation.

Elastic-plastic characterization

The shear tests in this work were operated by DMA, which has its capability limitation. The maximum force is too low to cause remarkable elastic deformation that it is a regret not to find Au-Sn elasticity parameters under different temperature conditions or with different microstructures. A fact has to be admitted that DMA is not designed for measuring hard and brittle metal alloy, when itself has complex iron clamp system that has comparable elastic modulus with tested samples. Larger tensile test platform with higher test force will be suggested to investigate other fundamental mechanical properties, and then use them in a competed reliability simulations.

Investigate microstructure effect on other properties

Being a die-attache material, other fundamentals of Au-Sn like electrical properties and thermal properties are also significant in its application, and are remain unknown in this work. It is interesting to investigate how microstructure variation can influence these properties, where key properties such as electrical conductance, thermal conductivity, coefficient of thermal expansion(CTE) are measured. Based on these investigations, product design can be even tailored as targeting to certain requirements.

Port characterization methodology to other materials

This work consists a complete methodology of viscoplastic properties characterization for Au-Sn solders, and it can be also ported to other materials including but not limited to new generation of Pb-free solder materials.

Bibliography

[1] B.-S. Lee, C.-W. Lee, and J.-W. Yoon, *Comparative study of au–sn and sn–ag–cu as die-attach materials for power electronics applications,* Surface and Interface Analysis (2016).

[2] W. Pittroff, G. Erbert, G. Beister, F. Bugge, A. Klein, A. Knauer, J. Maege, P. Ressel, J. Sebastian, R. Staske, *et al.*, *Mounting of high power laser diodes on boron nitride heat sinks using an optimized au/sn metallurgy,* IEEE Transactions on Advanced Packaging **24**, 434 (2001).

[3] G. S. Matijasevic, C. C. Lee, and C. Y. Wang, *Au-sn alloy phase diagram and properties related to its use as a bonding medium,* Thin Solid Films **223**, 276 (1993).

[4] D. Ivey, *Microstructural characterization of au/sn solder for packaging in optoelectronic applications,* Micron **29**, 281 (1998).

[5] T. B. Massalski, H. Okamoto, P. Subramanian, L. Kacprzak, and W. W. Scott, *Binary alloy phase diagrams*, Vol. 1 (American society for metals Metals Park, OH, 1986).

[6] A. He, B. Djurfors, S. Akhlaghi, and D. G. Ivey, *Pulse plating of gold-tin alloys for microelectronic and optoelectronic applications,* Plating and Surface Finishing **89**, 48 (2002).

[7] Z. Ling, N. S. Ching, L. Zheng, F. S. Nong, T. Nguty, E. de Bruin, A. Xiao, and H. Thoonen, *Development of advanced ausn alloy plating technology for semiconductor application,* in *Electronic Packaging*

Technology (ICEPT), 2014 15th International Conference on (IEEE, 2014) pp. 113–116.

[8] S. Nakahara, R. McCoy, L. Buene, and J. Vandenberg, *Room temperature interdiffusion studies of au/sn thin film couples,* Thin Solid Films **84**, 185 (1981).

[9] J.-W. Yoon, H.-S. Chun, and S.-B. Jung, *Reliability analysis of au–sn flip-chip solder bump fabricated by co-electroplating,* Journal of materials research **22**, 1219 (2007).

[10] T. Namazu, H. Takemoto, and S. Inoue, *Tensile and creep characteristics of sputtered gold-tin eutectic solder film evaluated by xrd tensile testing,* Sens. Mater **22**, 13 (2010).

[11] J. Sigelko, S. Choi, K. Subramanian, J. P. Lucas, and T. Bieler, *Effect of cooling rate on microstructure and mechanical properties of eutectic sn-ag solder joints with and without intentionally incorporated cu 6 sn 5 reinforcements,* Journal of Electronic Materials **28**, 1184 (1999).

[12] M. Kerr and N. Chawla, *Creep deformation behavior of sn-3.5 ag solder at small length scales,* Jom **56**, 50 (2004).

[13] L. Yang, J. Ge, H. Liu, L. Xu, and A. Bo, *Effect of cooling rate on the microstructure and mechanical properties of sn-1.0 ag-0.5 cu–0.2 batio3 composite solder,* Journal of Electronic Materials **44**, 4595 (2015).

[14] K. Subramanian and J. Lee, *Effect of anisotropy of tin on thermomechanical behavior of solder joints,* Journal of Materials Science: Materials in Electronics **15**, 235 (2004).

[15] D. Grivas, K. Murty, and J. Morris, *Deformation of pb-sn eutectic alloys at relatively high strain rates,* Acta Metallurgica **27**, 731 (1979).

[16] A. Telang, T. Bieler, J. Lucas, K. Subramanian, L. Lehman, Y. Xing, and E. Cotts, *Grain-boundary character and grain growth in bulk tin and bulk lead-free solder alloys,* Journal of Electronic Materials **33**, 1412 (2004).

[17] G. Zhang, H. Jing, L. Xu, J. Wei, and Y. Han, *Creep behavior of eutectic 80au/20sn solder alloy,* Journal of Alloys and Compounds **476**, 138 (2009).

[18] F. H. Norton, *The creep of steel at high temperatures*, 35 (McGraw-Hill Book Company, Incorporated, 1929).

[19] D. May, A. Gordon, and D. Segletes, *The application of the norton-bailey law for creep prediction through power law regression,* in *ASME Turbo Expo 2013: Turbine Technical Conference and Exposition* (American Society of Mechanical Engineers, 2013) pp. V07AT26A005–V07AT26A005.

[20] L. Bråthe and L. Josefson, *Estimation of norton-bailey parameters from creep rupture data,* Metal Science (2013).

[21] M. S. Yeh, *Evaluation of the mechanical properties of a ternary sn-20in-2.8 ag solder,* Journal of electronic materials **31**, 953 (2002).

[22] S. Vaynman, G. Ghosh, and M. Fine, *Effects of palladium and solder aging on mechanical and fatigue properties of tin-lead eutectic solder,* Journal of electronic materials **27**, 1223 (1998).

[23] J. Elmer and R. Mulay, *Superplastic creep of ausn eutectic solder alloy,* Scripta Materialia **120**, 14 (2016).

[24] O. D. Sherby and J. Dorn, *Anelastic creep of polymethyl methacrylate,* Journal of the Mechanics and Physics of Solids **6**, 145 (1958).

[25] F. Garofalo, *Fundamentals of creep and creep-rupture in metals* (Macmillan, 1965).

[26] Y. Liu, J. Teo, S. Tung, and K. Lam, *High-temperature creep and hardness of eutectic 80au/20sn solder,* Journal of Alloys and Compounds **448**, 340 (2008).

[27] F. R. Larson and J. Miller, *A time-temperature relationship for rupture and creep stresses* (publisher not identified, 1952).

[28] S. Manson and A. Haferd, *Time-temperature,* (1953).

[29] F. C. Monkman and N. J. Grant, *An empirical relationship between rupture life and minimum creep rate in creep-rupture tests,* in *proc. ASTM*, Vol. 56 (1956) pp. 593–620.

[30] L. Anand, *Constitutive equations for the rate-dependent deformation of metals at elevated temperatures,* Journal of engineering materials and technology **104**, 12 (1982).

[31] M. Amagai, M. Watanabe, M. Omiya, K. Kishimoto, and T. Shibuya, *Mechanical characterization of sn–ag-based lead-free solders,* Microelectronics Reliability **42**, 951 (2002).

[32] J.-W. Kim and S.-B. Jung, *Experimental and finite element analysis of the shear speed effects on the sn–ag and sn–ag–cu bga solder joints,* Materials Science and Engineering: A **371**, 267 (2004).

[33] M. Motalab, Z. Cai, J. C. Suhling, and P. Lall, *Determination of anand constants for sac solders using stress-strain or creep data,* in *Thermal and Thermomechanical Phenomena in Electronic Systems (ITherm), 2012 13th IEEE Intersociety Conference on* (IEEE, 2012) pp. 910–922.

[34] M. Hutter, F. Hohnke, H. Oppermann, M. Klein, and G. Engelmann, *Assembly and reliability of flip chip solder joints using miniaturized au/sn bumps,* in *Electronic Components and Technology Conference, 2004. Proceedings. 54th*, Vol. 1 (IEEE, 2004) pp. 49–57.

[35] A. Yu, N. Khan, G. Archit, D. Pinjala, K. C. Toh, V. Kripesh, S. W. Yoon, and J. H. Lau, *Fabrication of silicon carriers with tsv electrical interconnections and embedded thermal solutions for high power 3-d package,* in *2008 58th Electronic Components and Technology Conference* (IEEE, 2008) pp. 24–28.

[36] M. Nishiguchi, N. Goto, and H. Nishizawa, *Highly reliable au-sn eutectic bonding with background gaas lsi chips,* IEEE transactions on components, hybrids, and manufacturing technology **14**, 523 (1991).

[37] M. Nishiguchi, *Method of adhesively and hermetically sealing a semiconductor package lid by scrubbing,* (1991), uS Patent 5,064,782.

[38] T. A. Tollefsen, A. Larsson, O. M. Løvvik, and K. Aasmundtveit, *Au-sn slid bonding—properties and possibilities,* Metallurgical and Materials Transactions B **43**, 397 (2012).

[39] K.-K. Wang, B.-H. Jiang, and D. Gan, *Orientation relationships of au 5 sn/au interfaces and formation sequence of au 5 sn and ausn at the au/sn interface,* Thin Solid Films **589**, 584 (2015).

[40] M. Sheen, C. Chang, H. Teng, J. Kuang, K. Hsieh, and W. Cheng, *The influence of thermal aging on joint strength and fracture surface of pb/sn and au/sn solders in laser diode packages,* Journal of electronic materials **31**, 895 (2002).

[41] K.-A. Lee, Y.-M. Jin, Y.-h. Sohn, J. Namkung, and M.-C. Kim, *Continuous strip casting, microstructure and properties of au-sn soldering alloy,* Metals and Materials International **17**, 7 (2011).

[42] C. C. Lee, C. Y. Wang, and G. S. Matijasevic, *A new bonding technology using gold and tin multilayer composite structures,* IEEE Trans-

actions on Components, Hybrids, and Manufacturing Technology **14**, 407 (1991).

[43] Q. Tan, C. Deng, Y. Mao, and G. He, *Evolution of primary phases and high-temperature compressive behaviors of as-cast ausn20 alloys prepared by different solidification pathways,* Gold Bulletin **44**, 27 (2011).

[44] M. Huang, Y. Yang, Y. Chen, and C. Dong, *Microstructure and mechanical properties of sn-rich au-sn solders designed using cluster-plus-glue-atom model,* Materials Science and Engineering: A **664**, 221 (2016).

[45] S. Anhock, H. Oppermann, C. Kallmayer, R. Aschenbrenner, L. Thomas, and H. Reichl, *Investigations of au-sn alloys on different end-metallizations for high temperature applications [solders],* in *Electronics Manufacturing Technology Symposium, 1998. IEMT-Europe 1998. Twenty-Second IEEE/CPMT International* (IEEE, 1998) pp. 156–165.

[46] F. Arabi, L. Theolier, T. Youssef, M. Medina, J.-Y. Deletage, and E. Woirgard, *Effect of voids on crack propagation in ausn die attach for high-temperature power modules,* in *Thermal, Mechanical and Multi-Physics Simulation and Experiments in Microelectronics and Microsystems (EuroSimE), 2017 18th International Conference on* (IEEE, 2017) pp. 1–6.

[47] R. Chromik, D. Wang, A. Shugar, L. Limata, M. Notis, and R. Vinci, *Mechanical properties of intermetallic compounds in the au–sn system,* Journal of materials research **20**, 2161 (2005).

[48] R. An, C. Wang, and Y. Tian, *Determination of the elastic properties of au5sn and ausn from ab initio calculations,* Journal of Electronic Materials **37**, 968 (2008).

[49] K. W. Seah, J. Hemanth, and S. Sharma, *Effect of the cooling rate on the dendrite arm spacing and the ultimate tensile strength of cast iron,* Journal of materials science **33**, 23 (1998).

[50] F. Ochoa, J. Williams, and N. Chawla, *The effects of cooling rate on microstructure and mechanical behavior of sn-3.5 ag solder,* JOM Journal of the Minerals, Metals and Materials Society **55**, 56 (2003).

[51] Z. Mei, J. Morris, M. Shine, and T. Summers, *Effects of cooling rate on mechanical properties of near-eutectic tin-lead solder joints,* Journal of Electronic Materials **20**, 599 (1991).

[52] S.-K. Seo, S. K. Kang, D.-Y. Shih, and H. M. Lee, *An investigation of microstructure and microhardness of sn-cu and sn-ag solders as functions of alloy composition and cooling rate,* Journal of electronic materials **38**, 257 (2009).

[53] H. Oppermann, M. Brink, O. Ehrmann, S. Groetsch, A. Plößl, A. Pfeuffer, N. von Malm, T. Groß, R. Fiederling, R. Kürschner, *et al.*, *A thermally enhanced bond interface for pixelated leds in adaptive front lighting systems,* in *Electronic System-Integration Technology Conference (ESTC), 2016 6th* (IEEE, 2016) pp. 1–7.

[54] S. Wiese and K.-J. Wolter, *Microstructure and creep behaviour of eutectic snag and snagcu solders,* Microelectronics Reliability **44**, 1923 (2004).

[55] I. Dutta, D. Pan, R. Marks, and S. Jadhav, *Effect of thermo-mechanically induced microstructural coarsening on the evolution of creep response of snag-based microelectronic solders,* Materials Science and Engineering: A **410**, 48 (2005).

[56] R. Sidhu, X. Deng, and N. Chawla, *Microstructure characterization and creep behavior of pb-free sn-rich solder alloys: Part ii. creep be-*

havior of bulk solder and solder/copper joints, Metallurgical and Materials Transactions A **39**, 349 (2008).

[57] R. Lagneborg and B. Bergman, *The stress/creep rate behaviour of precipitation-hardened alloys,* Metal Science **10**, 20 (1976).

[58] T. Zhou, T. Bobal, M. Oud, and J. Songliang, *Au/sn solder alloy and its applications in electronics packaging,* Coining Inc (1999).

[59] X. Fan, M. Pei, and P. K. Bhatti, *Effect of finite element modeling techniques on solder joint fatigue life prediction of flip-chip bga packages,* in *Electronic Components and Technology Conference, 2006. Proceedings. 56th* (IEEE, 2006) pp. 9–pp.

[60] A. Dasgupta, C. Oyan, D. Barker, and M. Pecht, *Solder creep-fatigue analysis by an energy-partitioning approach,* ASME Journal of Electronic Packaging **114**, 152 (1992).

[61] H. Akay, N. Paydar, and A. Bilgic, *Fatigue life predictions for thermally loaded solder joints using a volume-weighted averaging technique,* TRANSACTIONS-AMERICAN SOCIETY OF MECHANICAL ENGINEERS JOURNAL OF ELECTRONIC PACKAGING **119**, 228 (1997).

List of Figures